Scientific Research Publishing

Open Journal of Geology, 2026, 16(7), 393-430
https://www.scirp.org/journal/ojg
ISSN Online: 2161-7589
ISSN Print: 2161-7570

Integrated Geophysical and Geotechnical Site Characterisation for Civil Infrastructure Development in Sekondi-Takoradi, Ghana

Asare Asante-Annor[1*], Ernest Nyamekye Addo[1], Kwaku Raymond Frimpong[1], Gbenga Moses Olayanju[2]

[1]Geological Engineering Department, University of Mines and Technology, Tarkwa, Ghana
[2]Department of Applied Geophysics, Federal University of Technology, Akure, Nigeria
Email: *aasante-annor@umat.edu.gh

How to cite this paper: Asante-Annor, A., Addo, E.N., Frimpong, K.R. and Olayanju, G.M. (2026) Integrated Geophysical and Geotechnical Site Characterisation for Civil Infrastructure Development in Sekondi-Takoradi, Ghana. *Open Journal of Geology*, **16**, 393-430.
https://doi.org/10.4236/ojg.2026.167021

Received: June 10, 2026
Accepted: July 27, 2026
Published: July 30, 2026

Abstract

An integrated geotechnical site characterisation was conducted in Sekondi-Takoradi, Southwestern Ghana, to evaluate subsurface conditions for a major institutional infrastructure development project. The investigation focused on evaluating the engineering integrity, shear strength, and ultimate bearing capacity of the foundation soils to support heavy structural loads. Additionally, the study aimed to delineate critical subsurface anomalies, weak zones, and adverse geological structures that could compromise structural stability or threaten foundation longevity. The geophysical method deployed involved the use of electrical methods involving electrical imaging and vertical sounding approaches complemented with the evaluation of the geotechnical parameters of subgrade in the site based on the assessment of soil's geotechnical indices and engineering qualities of soil samples from five trial pits from the study. Based on the results of resistivity imaging carried out using the Schlumberger dipole-dipole configuration along four traverses, the lithologic profiles of the subsurface geology revealed weathering prognosis depicting three lithologic layering characteristics of highly resistive and very thin topsoil (ferruginous sandstone/lateritic soil); intermediate highly resistive sandstone and underlying bedrock, while 1D geoelectric profiles also revealed highly resistive four lithologic units which conformed well with the 2D resistivity tomographic expressions of geologic sections in the area. The overburden thickness is usually less than 5 m, an indication that the subgrades are generally not up to 5 m in thickness. The 2D resistivity structures suggest that the subgrade materials are highly compacted in collaboration with the 1D resistivity profiles that are diagnostic of highly compacted and acidic sediments that usually possess extremely high resistivity values. Features within the subgrades are typified by undulating surfaces and fractured layers with local depressions at some parts of the site. Based on derived geophysical parameters, the subgrade could be rated as low to moderate integrity to support high load capacity. However, some parts are characterised by weak lateritic soils often associated with seepage paths that are recognised as near-surface fractures or joints in the areas. Such weak zones can have an impact on the bearing capacity of the subsoils; thus, proper measures must be considered before engineering works commence. The soil profiles revealed that the upper layers on the hilly parts of the study area are characterised by dry, loose, and coarse-grained sand, while the lower layer was discovered to be primarily residues from the parental bedrock made of reddish brown and loose fine-grained sandy clay, indicating deep weathering of leached bedrock. However, the upper sections of the slope area were revealed to be transported materials down the hill at the site. The subgrade materials exhibit specific gravity ranging from 2.69 to 2.70 g/cm^{-3}, an indication that the soil is rich in quartz., while the ultimate bearing capacity of the subgrades is between 1552.7 kN/m^2 and 1281.7 kN/m^2, which suggests that the subgrades can withstand allowable pressures between 480.6 kN/m^3 and 410.3 kN/m^3 without failure within the area.

Keywords

Geotechnical Site Characterisation, Electrical Resistivity Imaging, Vertical Electrical Sounding, Subsurface Anomaly Detection, Sekondi-Takoradi

1. Introduction

The School of Railways and Infrastructure Development (SRID) is a specialized faculty of the University of Mines and Technology (UMaT), established to advance Ghana's technological and industrial education. It is situated at Essikado, Takoradi, in the Western Region of Ghana. As part of a developmental plan to impact the host community and the entire Western Region of Ghana, SRID proposed a satellite Faculty to be located at Sofokrom, Sekondi Takoradi, Ghana.

A site investigation has to be structured to acquire all possible information that could be gathered through a proper understanding of the subsurface condition and probable foundation behaviour [1] [2]. Thus, site investigation will allow information such as the nature and sequence of strata, the groundwater conditions at the site, the physical properties of the soil and rock underlying the site, and the mechanical properties of different soil or rock strata to be acquired to ensure the success of engineering constructions plans.

Civil construction of infrastructures requires as a matter of compulsion, geotechnical studies to characterise and evaluate the subsurface parameters to establish competency and load-bearing capacity of the soils that intend to serve as foundation materials of intending dead and loads within the site. As part of the construction plan, a comprehensive pre-foundation study will include geophysical and geotechnical studies of the proposed site, which can be achieved through integrated approaches that can involve various geologic engineering and geophysical methods designed for foundation studies in civil engineering works and hydrological nature of the site [3]-[6]. Details of these methods have been described in texts and presented by various authors [7]-[10].

This paper presents the details of pre-foundation studies carried out at the proposed site designated for the satellite faculty of SRID, Ghana at Sofokrom (a suburb of Essikado) using an integrated approach involving the application of the geophysical method and engineering geologic methods. Thus, the work carried out focused on the engineering characteristics of the site in terms of its natural load-bearing capacity and integrity to serve as suitable foundation materials for civil engineering structure design and construction.

The geophysical approach applied in this work involved the application of the electrical resistivity method by adopting: 1) the electrical imaging technique, which is in an actual sense an application of the Combined Horizontal Profiling and Vertical Resistivity method for a 2-dimensional characterisation of resistivity variation within the probed section of the soil and 2) the Vertical Electrical Sounding (VES) method that can be used to view 1-dimensional delineation of the lithologic sequence of the soil in the area [8] [10] [11]. From the use of these geophysical methods information including the spatial pattern of soil properties, protective capacity of the soil, hydrological condition, depth to water table, internal structural deposition, and presence of hazardous geologic features (such as joints/fracture/fault and seepage paths) that can lead to feature failure of infrastructure constructed in the site were provided to assist in pre-foundation decision making for various infrastructures to be constructed at the site. Integration of geophysical and spatial analyses of scattered geotechnical data interpolation allows for improvement in the accuracy of decision-making for proper civil engineering structure design and construction [12].

Electrical Resistivity Imaging (ERI) is a geophysical technique that is normally used to delineate the earth's subsurface condition, such as the subsurface thickness, rock structure, groundwater flow and aquifer, groundwater salinity, and mineral exploration [13] [14]. The method generally allows the interpreter to produce a 2D profile or resistivity structure of subsurface conditions based on the resistivity value of subsurface materials. Electrical imaging is a surveying technique mostly used for an area of complex geology where the use of resistivity sounding and other techniques is not appropriate for providing detailed subsurface information in the area under study [15]-[17]. In addition, geotechnical tests were conducted to derive soil parameters that are appropriate in decision making for a developmental program of infrastructures at the site in terms of competency or integrity and bearing capacity of the overburden materials (subgrades) to support heavy loads, as well as possible areas that might be prone to failures in future.

2. Study Description and Geological Setting

2.1. Study Description

The proposed site for SRID satellite Faculty is located at Sofokrom north of

Mpentsem, a town situated within Sekondi-Takoradi District in the Western Region of Ghana, formerly Shama Ahanta East District having its capital at Sekondi [18]. Sofokrom is about 26.6 km from the centre of Takoradi and about 16 km to Sekondi, the Western region's capital. It extends between Latitude 4˚59'12.74"N - 4˚59'57.17"N from south to the north of the equator, and lies within Longitude 1˚41'31.98"W - 1˚41'50.44"W to the east to the west of Greenwich meridian (**Figure 1**). It has been discovered that the landscapes of the Sekondi and Takoradi Metropolis are generally characterised by low-lying planes mostly with an altitude of 6 m above sea level, but are interspersed with ridges and hills ranging from 30 - 60 m high [19]. The topography of the coast has been reported to be affected by a series of fault systems [20]. However, the physiography of the study area shows that the landscape is characterised by a ridge (**Figure 2**) with highly resistant and acid topsoil due to heavy leaching, with shrubs and altitude rising from 24 m to about 64 m above sea level (**Figure 3**). **Figure 4** shows the ground surface relief of the area as a digital elevation model.

The Sekondi-Takoradi District has been known to have three main vegetation types: mangrove, savannah woodland, and tropical forest. The tropical forest in which Sofokrom is situated is predominately found around the northern parts of the district [21]. The savannah woodland is dotted around the middle belt, while the mangrove vegetation is found along the southern portion [21].

The district also lies within the south-western equatorial zone that experiences fairly uniform temperature, ranging between 22˚C and 28˚C in August and March. The metropolis also enjoys two periods of rainy seasons with a mean annual rainfall of about 2350 mm [22]. The major rainfall occurs between March and July, while the minor rainfall occurrence is between September and October. The dry season occurs for the rest of the year, while relative humidity is generally high throughout the year ranging between 50% and 70% in the dry season and 75% and 85% in the wet season [22].

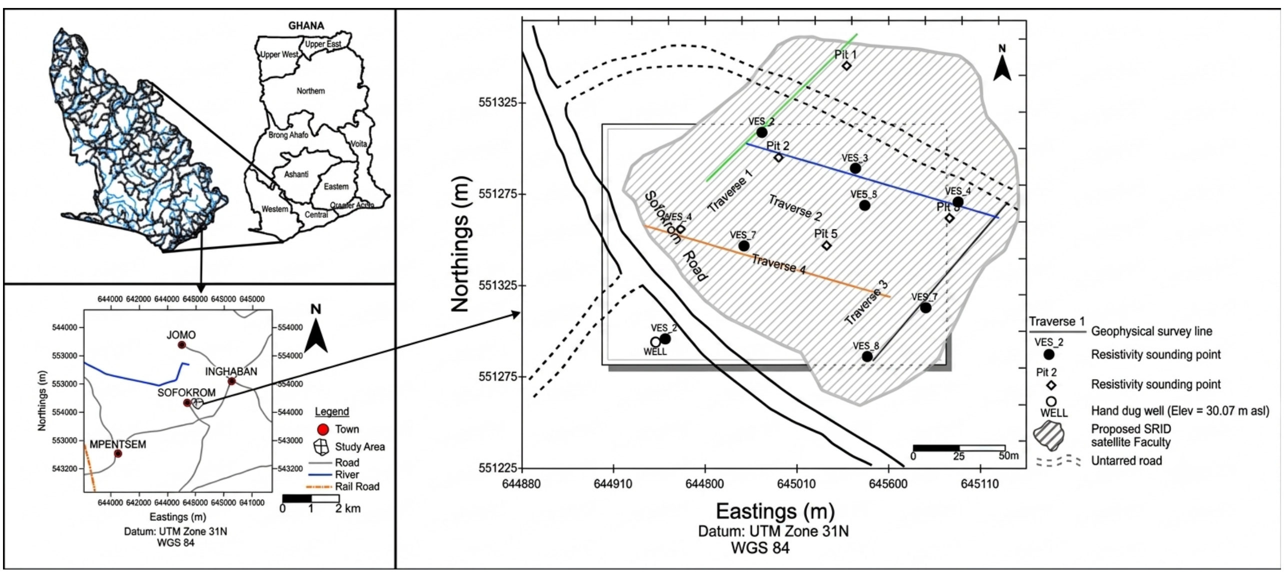

Figure 1. Location map and field layout of the study area.

Figure 2. Physiography of the area showing a ridge with shrubs.

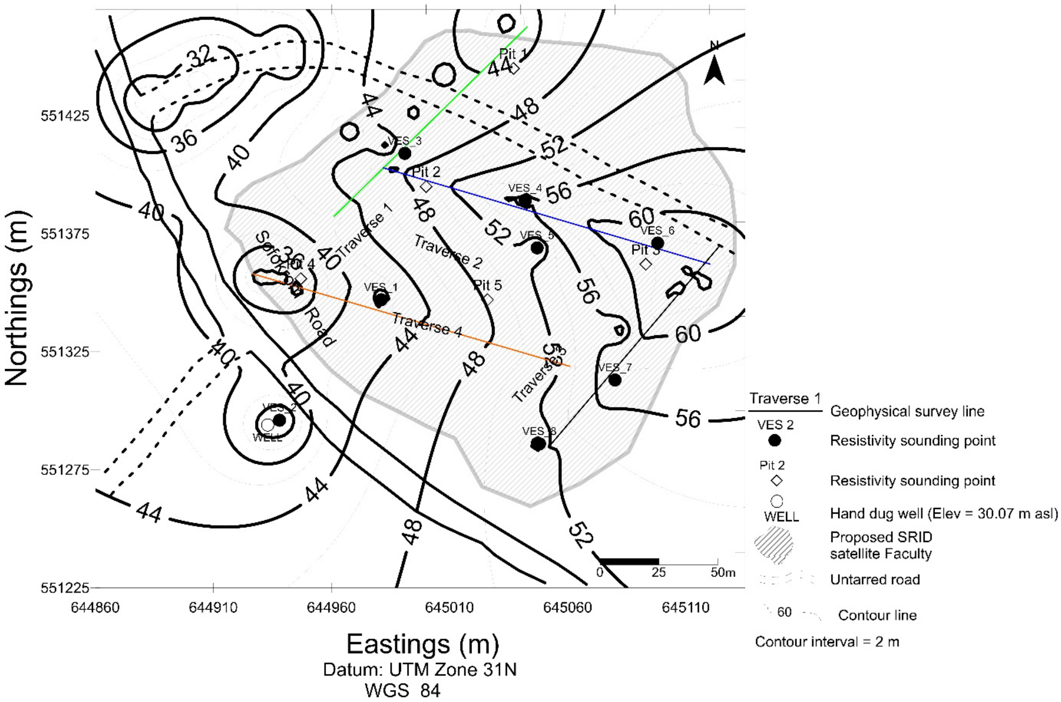

Figure 3. Topographic map of the study area.

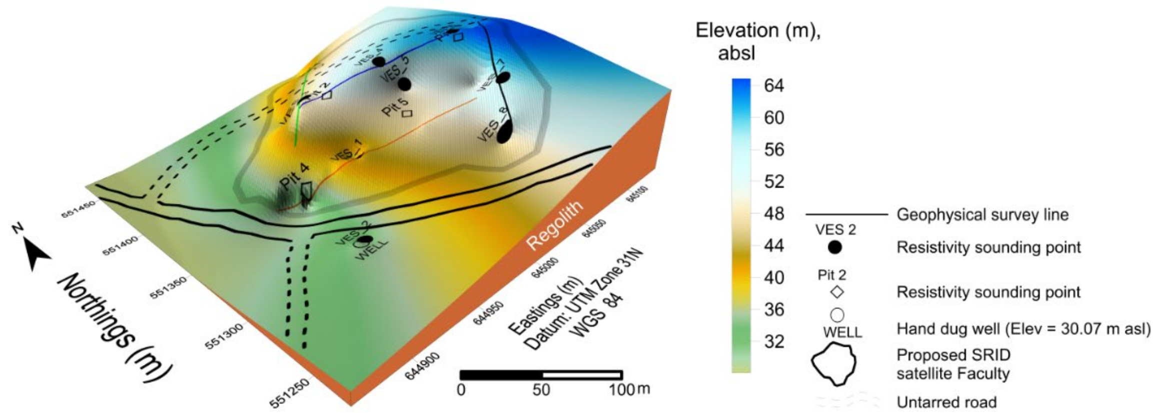

Figure 4. Digital elevation model of the study area.

2.2. Geological Setting

Sekondi-Takoradi is underlain by a crystalline basement of Dixcove and Cape Coast granites, unconformably overlain by the sedimentary Sekondian Group. This group comprises seven formations, Ajua Shale, Elmina Sandstone, Takoradi Sandstone, Takoradi Shale, Effia Nkwanta Beds, Sekondi Sandstone, and Essikado Sandstone. The sedimentary environment has been interpreted to be of non-marine to coastal marine facies [20] [23]. It was postulated that Paleoweathering in the source area, therefore, is one of the most important processes affecting the composition of sedimentary rocks [23].

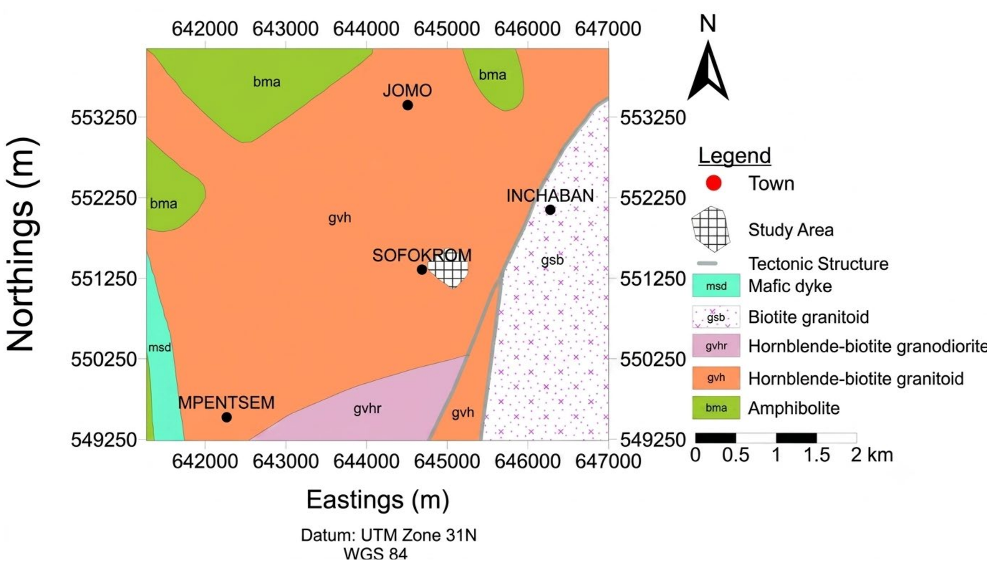

Figure 5. Simplified geological map of the Sekondian group in the Sekondi Takoradi area, Ghana (after [20]).

Most of the rocks are mainly found in Diabenekrom, Essipon, Kojokrom, and Butumajebu, with the Late Ordovician to Lower Cretaceous Sekondian Group outcropping along the west and central coast of Ghana [24]. The Sekondian Group is located in a deep unconformity in the Birimian supergroup of granitic rocks in the Paleoproterozoic. Provenance studies have shown that the sedimentary rocks of the Sekondian Formation are mainly derived from Birimian granites [25]. The Birimian terranes are a mix of metamorphosed volcanic, sedimentary, and plutonic rocks and low-grade metavolcanic and metasediments with almost half of the terranes consisting of alkaline granites. The study area (**Figure 5**), centered around Sofokrom, is dominated by hornblende-biotite granitoid (gvh), which forms the most extensive lithological unit across the mapped area, extending from the northern boundary down through the central and western portions of the map. Bordering this to the south is a band of hornblende-biotite granodiorite (gvhr), a distinct but related intrusive unit. To the east, the area transitions into a biotite granitoid (gsb) unit, mapped with a stippled texture, which lies close to the town of Inchaban. Patches of amphibolite (bma), a mafic metamorphic rock, occur in the northern part of the map near Jomo, while a narrow strip of mafic dyke (msd) intrudes along the western edge near Mpentsem. A tectonic structure (fault or shear zone, shown as a grey line) runs roughly north-south through the eastern part of the map, separating the granitoid unit from the biotite granitoid to the east. According to [26], within the Sekondi-Takoradi, areas underlain by hornblende-biotite granitoid and hornblende-biotite granodiorite exhibit very high susceptibility to slope instability. This underscores the geotechnical significance of these lithological units for infrastructure development in the region. These rocks believed to be from the Birimian Structural Unit occupy most of the highlands and they are observed to be undulating (**Figure 2**). The soils in the area are deep, open, and acidic in many places due to heavy leaching of bases from the top because of the high rainfall, humidity, and temperature [27].

3. Materials and Method

Materials deployed in the study include mainly the PASI resistivity meter and field accessories for the geophysical survey used in the electrical imaging and vertical electrical soundings at the site (**Figure 6**) and laboratory tools for geotechnical analyses including Casagrande cup, palette knife, moisture containers, oven, weighing balance, grooving tool, glass plate and sieves of different aperture size (0.425 - 0.70 mm) (**Figure 7(a)** and **Figure 7(b)**).

A reconnaissance survey was carried out by carrying out preliminary demarcation of the proposed Faculty site using a hand-held GERMAIN 12 Global Positioning System (GPS) to obtain coordinates of data points for the geophysical surveys conducted and establish azimuth of the four traverses used in acquiring electrical resistivity data. A topographic contour map of the area was acquired from the Survey and Geo-informatic Department of SRID.

The coordinates of the hand-dug five trial pits randomly distributed within the site were also obtained using the GPS, with the depth made to a maximum of 1.3 m. These representative soil samples were labelled appropriately and sent to UMaT Geotechnical Laboratory for the following analysis: Atterberg limits, specific gravity, soil particle grades, and direct shear strength.

Figure 6. PASI resistivity meter and ancilliaries.

(a) (b)

Figure 7. (a) Casagrande cup used for the Atterberg test and (b) A sieve stack on a mechanical shaker.

3.1. Geophysical Survey

Relying on the information for the need for the derivation of physical parameters of the geologic disposition of the area in terms of geotechnical and hydrological significance, the geophysical survey was designed to cover both hydrological and geotechnical indicators from the geophysical data acquisition, thus the use of both Schlumberger array designed electrical tomographic and vertical electrical sounding methods described below.

3.1.1. Electrical Resistivity Imaging

Field data acquisition employing the aid of a dipole-dipole array is one of the approaches to conducting Electrical Resistivity Imaging (ERI) within an area using four electrodes, as displayed in **Figure 8**. A dipole of current electrodes labelled A and B is separated by a distance, "a", in a similar manner with the potential electrodes labelled M and N also separated by the same distance "a". The centre of the dipole is increased while measurements of apparent resistivity data are obtained at regular intervals along the profile, with a gradual increase in the dipole spacing. The primary reason for the sequential increase in the distance between dipoles as a multiple of “a” is to allow for an increase in the depth of investigation and to obtain a 2D distribution of points of observation.

The Electrical Resistivity Tomography (ERT) data acquisition was carried out with the aid of the PASI resistivity meter and its ancillaries along four traverses with profile-length varied from 100 - 200 m across the study area. As the measurements progress, the spacing between the dipole electrodes “a” remained fixed, but the dipole distance is varied as multiple of the spacing (expansion factor), *i.e.*, “na”, where “n” is varied from 1 - 5, while “a” remains fixed at 5 meters as the space between each electrode pair (Figure 9).

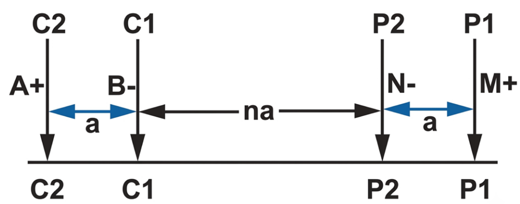

Figure 8. Instrumental arrangement for Schlumberger dipole-dipole array.

Figure 9. Field arrangement for Schlumberger dipole-dipole resistivity survey.

The geometric factor for the Dipole-dipole is expressed as:

$$k = n\pi(n+1)(n+2)a \quad (1)$$

where "n" is the spacing factor and "a" is the electrode spacing used for the particular measurement. The apparent resistivity value (ρ_a) for each "n" value was calculated by multiplying the resistance (*i.e.*, resulting voltage drop divided by the current obtained) with the geometric factor associated with the "n" values using the Ohm's law presented in (Equation (2)):

$$\rho_a = \frac{kV}{I} \quad (2)$$

where I = current flow, V = voltage, and k is the geometric factor that is determined by the electrode arrangement using (Equation (1)).

Data are generally presented as a pseudo section of the raw data, which is usually compared with the theoretical pseudo section for quality check for the cleanness of the raw data and qualitative analysis. However, the final results in terms of processed images, which are the inverted field data using the DIPRO for Windows (DIPROfWin) version 4.0 software, are presented as resistivity tomographic displays or resistivity structures (tomographic imaging) as described by [10] [28].

The inversion was based on Finite Difference Modelling (FDM) for topography treatment. The output produced as Electrical Resistivity Tomography (ERT) of the subsurface in the area aids the assessment of the geology of the site by providing both lateral and vertical information about the study area. The pseudo sections of the raw and synthetic data show an interpretation of unilateral data, while a close semblance of the contour maps is an indication of the noise-to-signal ratio or neatness of the acquired field data.

3.1.2. Vertical Electrical Sounding

Despite details of geologic features that can be expected from the tomographic display of resistivity structure in the area, a quick assessment of the lithologic units vertically can be achieved with the use of electrical sounding data, which predate resistivity imaging and are often employed as a hydro-geophysical tool for lithologic characterisation. The locations of the five trial pits and eight VES stations were selected to provide representative coverage of the major geomorphic units across the site, including the hilly terrain, slope sections, and local depression zones. This sampling strategy enabled the integrated geophysical and geotechnical datasets to capture the spatial variability of subsurface conditions and facilitated correlation between electrical resistivity responses and engineering soil properties. The vertical soundings were conducted based on the analyses of electrical imaging that were used to infer areas that show local increases in water contents that are characteristic of hydrological significance or possible weak zones. Strategically, eight (8) Vertical Electrical Soundings (VES) were carried out with the aid of a Schlumberger array designed such that the spread length (AB) varies from 130 to 450 m, while the electrode spacing of the inner potential electrodes ($r = MN$)' separation was frequently changed using the rule of thumb $S > 5r$, where ($S = AB/2$) the half-spacing for the current electrodes (**Figure 10**).

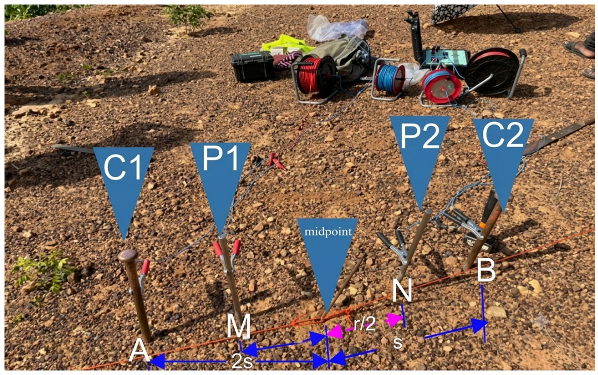

Figure 10. Field arrangement for the VES-Schlumberger array.

The measured soil resistance through the resistivity meter was later converted to apparent resistivity ρ_a by multiplying the geometric factor (k) for Schlumberger used with the measured resistance R using Ohmic law (Equation (2)), with the geometric factor for Schlumberger VES design expressed as:

$$k = \pi \frac{\left(s^2 - r^2\right)}{r} \tag{3}$$

where "s" is the half-distance between A and B current electrodes and "r" is the electrode spacing between M and N potential electrodes in any particular measurement.

The Vertical Electrical Sounding (VES) allows a deeper depth of investigation to achieve; however, the topography and the built-up areas reduce the spread length that can allow for greater penetration in the area. The variation of resistivity with depth was determined using a semi-quantitative approach, whereby the partially interpreted field data were later subjected to inverse modelling with the aid of the DCInv™ computer program. The output models were presented as characteristic layer effective resistivity and depths.

3.2. Geotechnical Investigation

A site investigation was carried out to determine the necessary input parameters that will help in the effective planning of the infrastructural development of the site. All five trial pits were excavated to the same maximum depth of 1.5 m to provide consistent subsurface information for engineering characterization across the study area. The primary objective of conducting the geotechnical tests was to obtain sufficient subsurface data to support architectural design and reliable determination of the types, locations, and principal dimensions of all major structures at the site. Disturbed samples of the materials were obtained from the site for laboratory testing to provide a basic knowledge of their engineering properties, such as the Atterberg limits (liquid limit, plastic limit, and plasticity index), particle size distribution, and the direct shear strength. These test results will provide a clue to the geomaterial present and a suitable framework for the soil log to sustain building construction at the site.

The following tests were carried out on the soil samples in the laboratory.

3.2.1. Atterberg Limit Test

The Atterberg limit tests were conducted based on the British BS 1377: Part 2 [29] standard protocol as described by [30] to establish limiting water contents that define the transition of the soil sample between the liquid, plastic, semi-solid, and solid states of fine-grained soils. Atterberg limits are a basic measure of a fine-grained soil's critical water content including Liquid Limits (LL), Plastic Limits (PL), and Plasticity Index (PI). The apparatus for determining these geotechnical indices is developed by [31] and the procedure for the test is called the Casagrande cup method.

1) Liquid Limit Test

The liquid limit is an intrinsic geotechnical property that can help in determining the soil integrity or competency as a foundation material. The liquid Limit Test conducted on the soil samples assists in determining the limiting water content at which the soil sample would pass from a liquid state to a plastic state or the water content at which the soil starts to behave like a plastic solid [32]. The liquid limit is determined from an apparatus that consists of a semispherical brass cup that is repeatedly dropped onto a hard rubber base from a height of 10 mm by a cam-operated mechanism [33].

Initially, before conducting the laboratory test, a 200 g of dry sample was sieved through a 0.425 mm diameter sieve onto the glass plate to remove coarser particles and portions of the sieved materials were reserved for the various tests conducted. A portion of the fine particles mixed with distilled water was made into a rolled thread of moist particles using the palette knife. The palette knife is then used to scoop the thick paste of the moist sample into the Casagrande cup and a groove is cut into the soil using a standard grooving tool. The crank operating the cam is turned anticlockwise until the groove is closed and the number of blows required to close the groove is counted and recorded. The container and its contents of pieces of the sample that flowed together are reweighed, and placed in the oven for 24 hours to determine the moisture content of the sample. The procedure can be repeated several times to achieve a lower count of blows.

2) Plastic Limit Test (PL)

The plastic limit test was conducted on the soil samples to determine the moisture content of the soil below which it transforms from plastic to a semi-solid state [32] [34].

A moist sample of each of the soil samples was made from the sieved portion made to pass through a 0.425 mm sieve and rolled into a thread of 3 mm diameter to a point at which it could no longer be rolled and broke as rolling continued. The threads were then placed in moisture content containers, weighed, and dried in an oven to determine the moisture content of the sample. The procedure was repeated three times and the values were recorded, while the moisture content was determined by subtracting the dry weight from the wet weight of the soil sample and dividing by the dry weight. The mean of the three moisture content tests, rounded off to the nearest whole number, is the plastic limit.

3) Plasticity Index (PI)

The plasticity index can be described as the range of moisture content at which the soil is plastic and is the difference between liquid limit and plastic limit values.

Once the liquid and plastic limits are determined, the PI can be calculated using the following expression:

$$\text{PI} = \text{LL} - \text{PL} \tag{4}$$

where LL is the liquid limit and PL is the Plastic limit.

The index is used to predict or assess the expansivity of the soil. The lower the plasticity of soil, the better the engineering property of the soil.

3.2.2. Particle Size Analysis (PSA)

The grain size distribution in an area provides information for the classification of soils for engineering purposes. The sieve analysis of the soil samples obtained at the site was conducted in conformity with the standard British protocol BS 1377: Part 2 [29] using the wet sieving separation technique. From each sample obtained from the pit, 500 g of the sample was weighed for each pit and soaked in water for an hour. The soaked samples were made to pass through both the 425 microns (0.425 mm) and the 750 microns (0.075 mm) while the sample was continuously mixed with water until the fine particles had completely passed and the water became clear. The residue of samples in the sieve is then poured into a container and oven-dried. The dried samples are then evenly reduced in size by the cone and quarter method. Sieving was performed using the cone and quarter method, whereby the sieves are stacked on the mechanical shaker and arranged in order of reducing aperture size with a receiving container at the base. The dried sample was placed on the top sieve, covered with a lid, and the whole set of sieves was agitated by the shaker. The retained soil particles on each sieve are then weighed and the percentage of retained particles is obtained using Equation (5):

$$\text{Percentage retained on sieve} = \left(\frac{\text{mass of soil retained}}{\text{total mass}}\right) \times 100\% \tag{5}$$

While,

$$\begin{aligned}&\text{Cumulative percentage retained on sieve}\\&= \sum \text{percentage retained on all coarse sieves}\end{aligned} \tag{6}$$

$$\text{Percentage finer} = 100\% - \text{cumulative percentage retained} \tag{7}$$

The plot of the percentage finer of the soil sample is then plotted on the log-log graph in order to classify the soil samples.

3.2.3. Specific Gravity Analysis (SGA)

The specific gravity values for the soil samples from the site are estimated using the British standard BS 1377:PART 2 [29] protocol. 50 g of dry samples taken from each layer from the trial pits were grinded and sieved through a 425-micron (0.425 mm) sieve. From the sieved particles, 12 g each was used in determining the sample's specific gravity. The empty relative density bottles used in the experiment were initially measured. The density bottle is then filled with water and its water-filled weight is recorded. The weighed soil sample was later filled with a dried density bottle and water was added to the brim. The bottle containing an over-saturated soil sample was then weighed and the mass recorded. The procedure was then repeated for samples from other layers.

The specific gravity (Gs) of the soil can be estimated from Equation (8) as:

$$\text{Specific Gravity }(\text{Gs}) = \frac{M_2 - M_1}{(M_4 - M_1) - (M_3 - M_2)} \tag{8}$$

where:

Gs = Specific gravity, M_1 = Mass of density bottle, M_2 = Mass of the bottle + dry soil, M_3 = Mass of the bottle + soil + water, and M_4 = Mass of the bottle + water only.

3.2.4. Direct Shear Test (DST)

The direct shear test was conducted on representative undisturbed soil samples obtained from trial Pits 3 and 4 in order to evaluate their shear strength parameters under applied shear loading. Trial Pits 3 and 4 were selected because they represent the two dominant geomorphic settings at the site, namely the hilly terrain and the slope/depression zone, respectively. Consequently, the test results provide representative engineering properties for the principal ground conditions encountered across the study area. In carrying out this test, a 60 mm × 60 mm cutting box was driven into the undisturbed sample from the trial pits that is forced into the experimental tube to obtain the sample for the test. The extracted sample was carefully put into the shear box to ensure that the ring fitted properly into the shear box apparatus. The gauge for the horizontal movement, vertical movement, and proving ring was adjusted to the zero (2500) mark. The beam jack was adjusted to be in contact with the lever-loading arm and the sample was subjected to the normal loads of 2.1 kg, 4.2 kg, and 8.5 kg. A shear force was then applied under each load and the shear stress was monitored until failure occurred. The sample was unloaded and weighed. The sample was later placed in the oven to dry and its dry weight was recorded. The procedure allows the displacement under shear load, the proving ring reading and settlement dial gauge to be recorded.

4. Discussion of Results

4.1. Geophysical Investigation

The various information provided from the results of geophysical investigations carried out is discussed on the integrity of the subsoil materials in terms of ability to support foundations for the construction of proposed infrastructures, hydrological characteristics, and identification of possible risks that can be posed by internal features in the subsurface at the study area.

4.1.1. Electrical Resistivity Imaging

The results of electrical resistivity imaging conducted along the four survey traverses are displayed as the tomographic display of the subsurface internal structures in a two-dimensional plan.

Characteristic Resistivity Imaging along Traverse 1

The results of processed field data and inverted resistivity structure along Traverse, conducted in the SW-NE direction, are displayed in **Figure 11**. The spread length of the traverse is 110 m, with the minimum dipole separation of 5 m as discussed in Section 3. Both the raw data and theoretical 2-D resistivity pseudo sections are shown in **Figure 11(a)** and **Figure 11(b)** respectively. The semblance in the two sections shows agreement in the resistivity pattern and a good correlation between the field and theoretical data, revealing undulating bedrock overlaid by highly resistive overburden with local depressions along the traverse. **Figure 11(c)** is the tomographic display of inverted field data after data point elevation has been incorporated. The characteristic electrical response from the subsurface diagnostic of a typical three-layer section reveals a moderately thick overburden of highly resistive topsoil and weathered layer. The bedrock is interpreted to comprise thick ferruginous sandstone, based on the high resistivity response together with observations from exposed outcrops within the gully along the eastern boundary of the site. Although electrical resistivity alone cannot uniquely determine lithology or engineering competence, this interpretation is strengthened by the geological exposures, trial pit logs and laboratory geotechnical results. The topsoil is very thin with thickness ranging from 0 - 0.5 m, rising above 45 - 46 m above sea level with resistivity usually above 2000 Ohm-m (yellowish to reddish colouration) on the 2D resistivity structure in **Figure 5**. The portion having an appearance of a bleeding point on the raw data recognised to be characterised by a relatively low resistivity zone between stations 8 and 9 (a distance of 40 - 45 m in the NE direction), was discovered to be characteristic of vertically linear features (usually cracks and joints) that extend through the intermediate layer into the bedrock. This was later realised to be a section through which surface water percolates into the ground and drains into the adjacent low land from the topsoil into the underlying layers.

The intermediate layer, which is sometimes exposed to the ground level and mimics the bedrock relief, has resistivity ranging from about 2000 - 20,200 Ohm-m with varying thicknesses between 0.5 m and 4.5 m. The base of this layer rises from 40 - 44 m above sea level. The linear features observed to extend from the topsoil into the layer and extending to the bedrocks are characteristic of cracks, joints, and fractures, which allow water to percolate into the medium and the underlying bedrock. The depressed zone within the area could also serve as water collection centres and may lead to the weakness of the foundation materials in the area. The bedrock is characterised by resistivity values greater than 200,000 Ωm, indicating a highly resistive formation that is interpreted to be relatively competent and extensively weathered or leached. Because resistivity is a non-unique geophysical property, this interpretation is supported by the geological observations and geotechnical test results rather than by resistivity values alone. However, the thickness of this layer cannot be established due to the limited depth of probe provided by the electrical array used. The maximum estimated thickness of the bedrock is approximately 17 m. The relatively high resistivity of the topsoil and intermediate layer suggests generally competent overburden materials. This interpretation is corroborated by the trial pit observations and laboratory geotechnical results, which indicate predominantly gravelly soils with favourable engineering properties. However, the bedrock relief and undulation of the topsoil require that proper cutting and filling of materials should be considered in designing the depth and type of foundation for structures intended to be erected at the site.

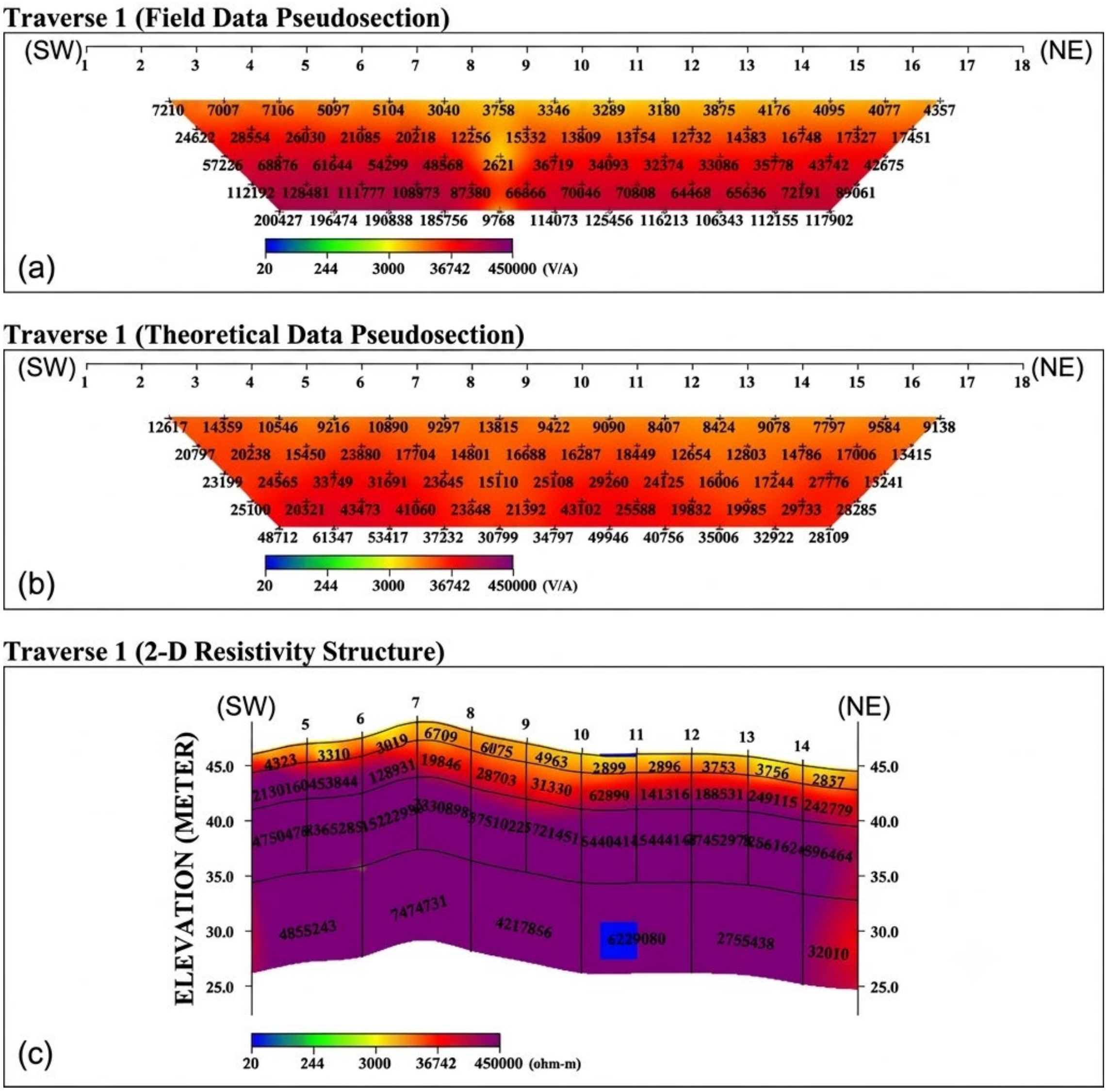

Figure 11. (a) Image display of field data pseudosection, (b) Theoretical data pseudosection and (c) Tomographic display of the 2D resistivity structure along traverse 1.

Characteristic Resistivity Imaging along Traverse 2

This traverse is along a steep landscape in a NW-SE orientation with a total distance of 140 m. Both the raw field and theoretically generated from the DI-PROfWinTM software are presented in Figure 12(a) and Figure 12(b) respectively, while the 2D resistivity structure of the inverted field data, shown as the tomographic display, is presented in Figure 12(c). Along the traverse, the topsoil has been deeply eroded due to the general southward depression of the landscape at the site. At the far end of the traverse is remnant of gravel being used in the construction of a building adjacent to the site. The inverted 2-D resistivity section revealed highly resistive topsoil with characteristic values between 10,000 Ohm-m, and 150,000 Ohm-m, except at the end of the profile with a resistivity of 132 Ohm-m on the raw data, which caused a reduction in resistivity value at the position of the deposited sand for ongoing construction in the area. It was observed that the impact of the sand body at a distance of 115 - 120 m caused a drastic reduction in the topsoil resistivity value, ranging from 1341 to about 1500 Ohm-m. The overburden is found to be about 1.5 - 2.5 m in thickness with the base lying between 47.5 m and 62.5 m, while the ground elevation varies from 52 - 64 m above sea level. Due to the almost absence of original soil residue along the traverse, the topsoil is highly thin with a thickness generally below 0.5 m. The weathered layer exhibits relatively high resistivity values that are consistent with comparatively dry and competent subsurface materials. However, resistivity alone cannot uniquely distinguish between the effects of moisture content, weathering, compaction and lithology, and therefore this interpretation is supported by the trial pit logs and laboratory testing. The bedrock is characteristically of high resistivity, having a range of values from 150,000 Ohm-m and above. Based on the generally high resistivity values, together with the observed soil profiles and laboratory test results, the overburden materials are interpreted to possess relatively good engineering competence and load-bearing capacity.

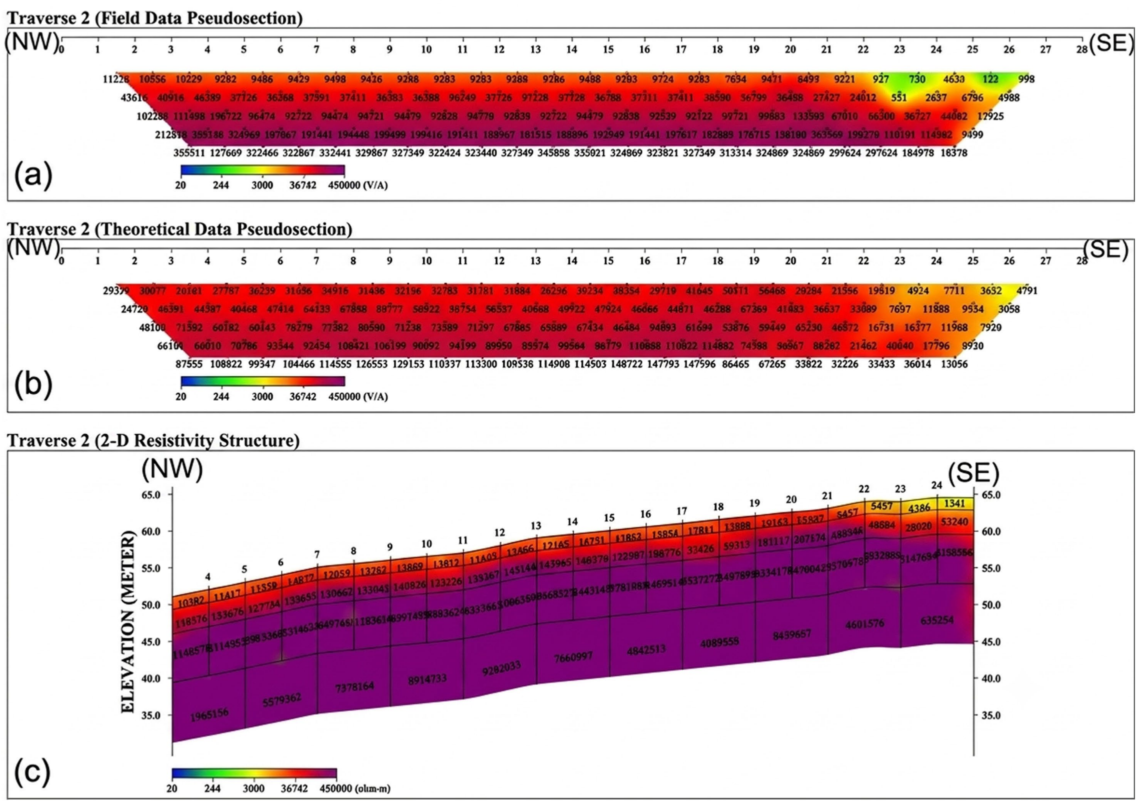

Figure 12. (a) Image display of field data pseudosection, (b) Theoretical data pseudosection and (c) Tomographic display of the 2D resistivity structure along traverse 2.

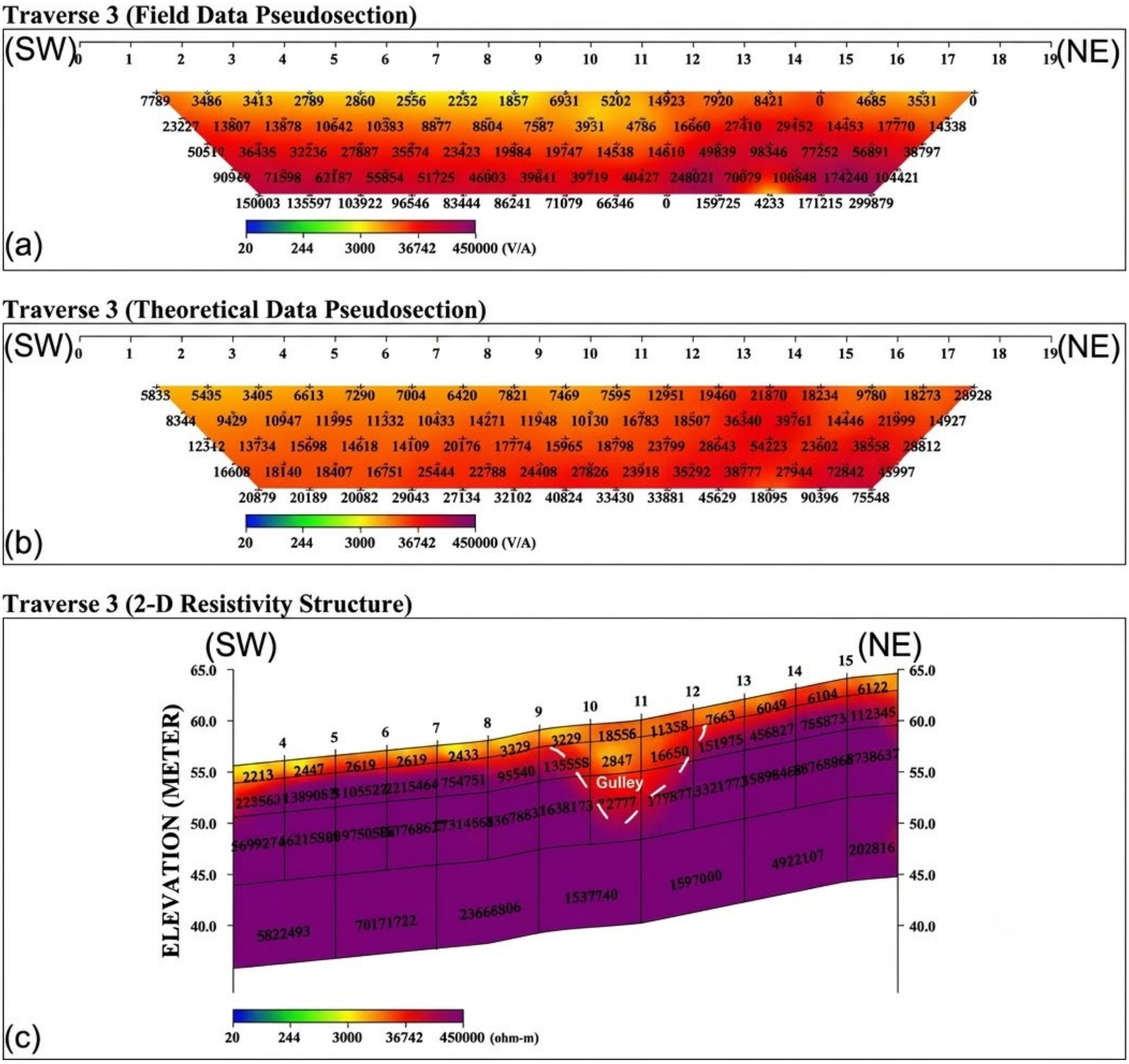

Figure 13. (a) Image display of field data pseudosection, (b) Theoretical data pseudosection and (c) Tomographic display of the 2D resistivity structure along traverse 3.

Characteristic Resistivity Imaging along Traverse 3

Traverse 3 was made parallel to Traverse 1 along SW-NE orientation with a spread length of 110 m. Both the raw field and theoretically generated have good correlation and semblance, as shown in Figure 13(a) and Figure 13(b), an indication of a high signal-to-noise ratio. The 2-D resistivity structure displayed in Figure 13(c) shows the topsoil characterised by highly varying resistivity ranging from 2213 - 18,558 Ohm-m, primarily of very thin ferruginous sandstone/lateritic soil. The topsoil thickness lies between 0 m and 0.6 m, while the ground level along the traverse ranges from 56 and 65 m above sea level. The intermediate layer is also relatively thin with a resistivity between 2847 Ohm-m and 200,000 Ohm-m. The thickness of this layer ranges from 0.2 - 6.2 m, while the deepest part is observed to be characterised by depression ("sand-filled gulley") with a maximum width of approximately 6 m. The resistivity value within this gulley is 2847 Ohm, with its centre at a distance of 52.5 m from the start of the traverse. The feature is believed to have formed a local discharge zone that might be responsible for the gulley to the west of the traverse within the site. The bedrock resistivity is very high, mostly above 200,000 Ohm-m with lithologic unit believed to be deeply leached and very sharp based on an observed section of mined overburden close to the site along the Takoradi-Cape Coast Highway. The base of the bedrock cannot be determined in the area due to the limited depth of investigation achieved from the spread length of the electrode array used. The generally high resistivity values, supported by the geological logs and geotechnical properties of the soils, indicate that the topsoil and intermediate weathered layers are generally suitable as foundation materials, except within the localized depression where seepage and reduced resistivity indicate weaker ground conditions. However, the weak zone that serves as a water discharging zone might pose a risk to the foundation of the structure erected at the site. Thus, there will be a need to cut and fill the subsoil materials in the area with the presence of a sand-filled void or discharge zone to enhance the stability of infrastructure that might be erected.

Characteristic Resistivity Imaging along Traverse 4

Traverse 4 has a NW-SE direction with a distance of 110 m within a depression zone within the site. The ground level along the traverse varies from 33.2 - 42.8 m. The pseudo sections for both the raw field and theoretical data displayed in Figure 14(a) and Figure 14(b) show a good correlation and a high signal-to-noise ratio. A zone of lower resistivity values dipping eastward was observed close to station 11 (55 m from the start of the traverse), which could be inferred to be a fractured zone. The 2-D resistivity section in Figure 14(c) indicates 2 - 3 geoelectric layering that can be categorised into the topsoil, intermediate layers, and bedrock; whereby the topsoil and intermediate layer have merged up in most places along the traverse. Generally, the topsoil is very thin, less than 0.5 m, and characterised by low resistivity ranging from 200 - 1000 Ohm. The topsoil is of slightly wet clayey sand with plantain trees and shrubs growing along the low land. This section is presumed to have been covered by materials washed down the slope along the gulley forming the zone of depression at the site.

The intermediate layer is usually characterised by resistivity less than 10,000 Ohm-m (238 - 4280 Ohm-m), which could be found to have merged with the underlying bedrock and has a thickness ranging from 0 - 0.5 m mostly. However, a zone of depression between stations 10 - 13 (55 - 65 m away from NW end) that serve as continuity of depressed zone observed along traverse 3 to the northeast of the profile is observed to have a thickness of approximately 10.0 m at the deepest point and is capped by ferruginous sandstone/lateritic soil of very high resistivity value (>100,000 Ohm-m). It was based on the local low resistivity zone that a well dug to the south within a building about 10 m away was located during the search for the lowering of resistivity in the area. The resistivity within the gulley ranges lies between 238 Ohm-m at the zone of saturation to 58,023 Ohm-m at the zone of aeration. The bedrock resistivity is characteristically high and varies from 2764 Ohm-m and above 100,000 Ohm-m. The comparatively low resistivity values along this traverse are interpreted to reflect increased moisture content associated with the shallow groundwater conditions and the local depression. Although moisture is the most likely controlling factor, resistivity is influenced by several subsurface properties; therefore, this interpretation is supported by field observations, the nearby well location and the geotechnical investigations. It was also observed along the traverse that the base of the bedrock has not been reached.

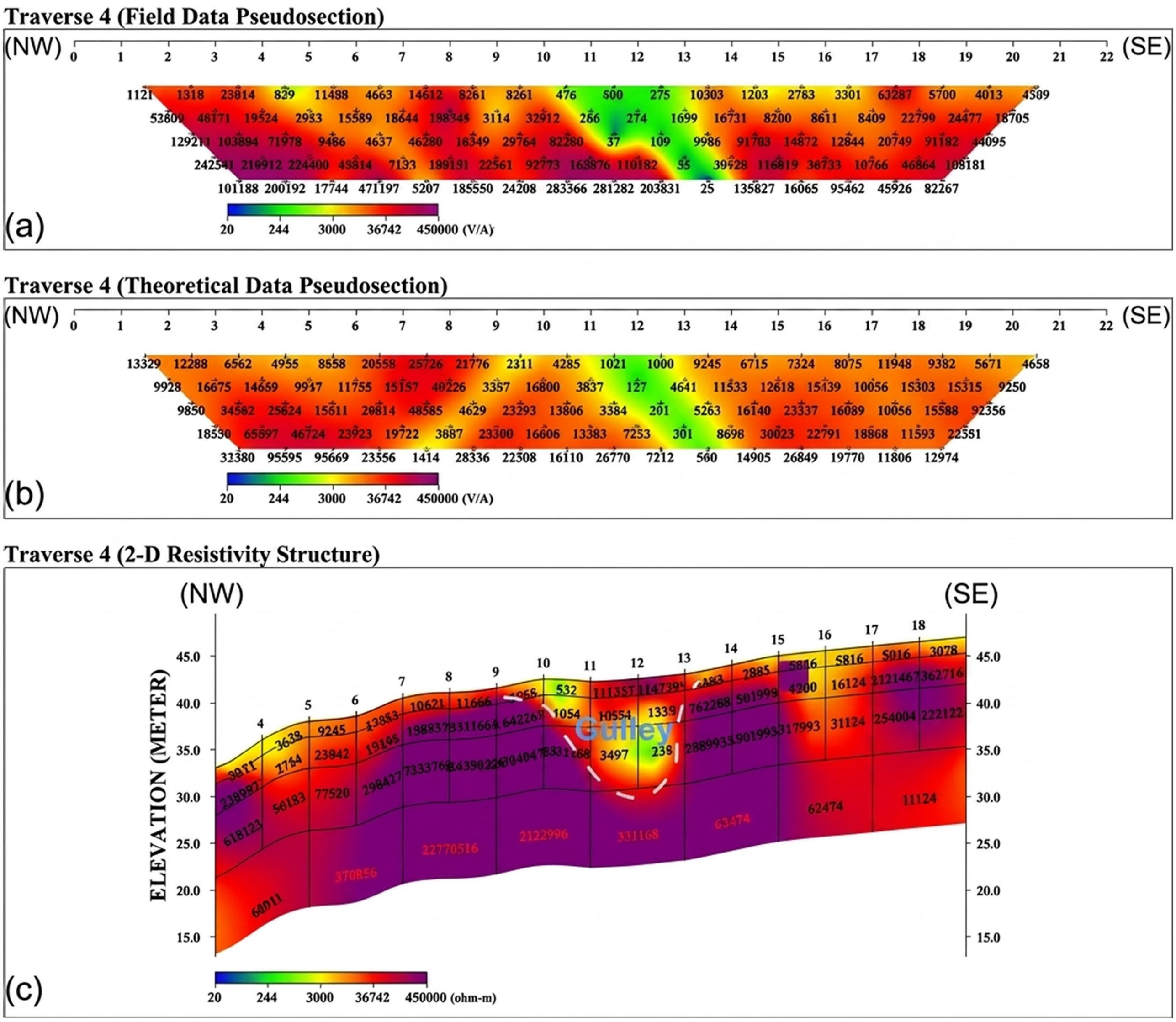

Figure 14. (a) Image display of field data pseudosection, (b) Theoretical data pseudosection and (c) Tomographic display of the 2D resistivity structure along traverse 4.

4.1.2. Vertical Electrical Sounding (VES)

To probe deeper at the site, the vertical electrical soundings undertaken at eight sounding points were interpreted and the lithologic profile under each of the VES' points was discussed in terms of characteristic layer resistivity and depth of investigation. Under VES 1 location (644981E/551347N, ELEV = 35 m), the interpreted sounding curve is characteristically an A-type Curve. The inverted resistivity curve, and its lithologic profile are shown in **Figure 15** whereby the result revealed a 4-layer 1D profile. The thin topsoil was observed to have effective layer resistivity of 693 Ohm-m characteristic of lateritic clay/ferruginous sandstone and thickness of 0.3 m. The second layer resistivity was estimated to be 35,203 Ohm-m while its thickness is estimated at 1.2 m. The third geoelectric layer has a thickness of 3.4 m with layer resistivity at 125,783 Ohm-m. Bedrock resistivity was estimated to be 981,616 Ohm-m, while the total depth is found to be 4.9 m. The lithologic profile was found to agree with the 2D resistivity profile along traverse 4, whereby the resistivity of the saprolite was detected to vary erratically and of increasing high value with depth.

The geoelectric profile in **Figure 16** shows lithologic sequence characteristics of parametric VES undertaken at the VES 2 location (644938E/551296N, ELEV = 33 m) beside the well at the opposite side of the road southward of traverse 4. The 1D geoelectric profile reveals a 4-layer model representing a KH-type curve whereby the resistivity rises from layer 1 to layer 2 but is reduced for layer 3 in contrast to the value at layer 2 before rising again for layer 4.

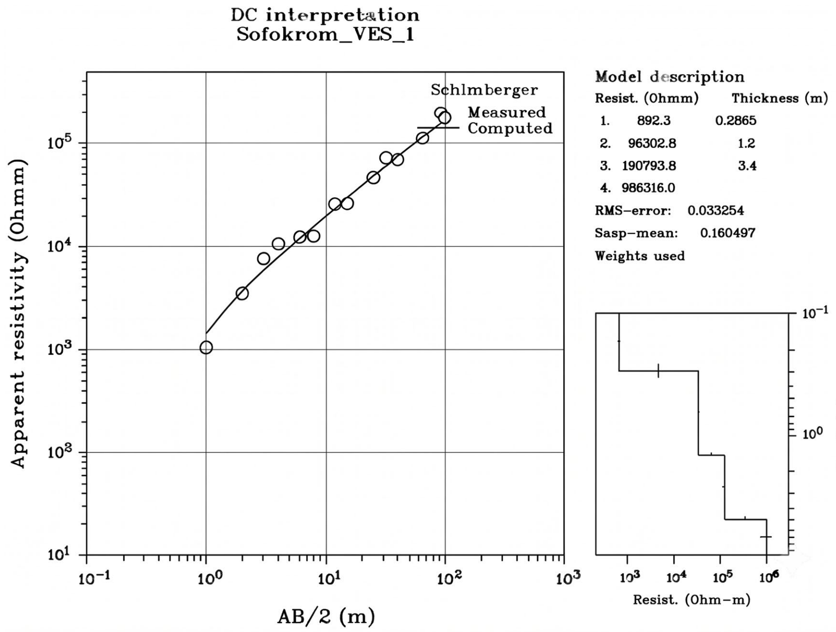

Figure 15. Depth sounding curve and 1D lithologic profile at VES_1 location.

The layer resistivity values are 116 Ohm-m, 63,059 Ohm-m, 7823 Ohm-m, and 784,931 Ohm-m for the topsoil, first substratum, second substratum, and the bedrock, while the thicknesses for the three layers overlying the bedrock are 0.16, 4.5

and 8.4 m respectively with total overburden put at 13.06 m. This trend of resistivity variation was similar to what was obtained along traverse 4.

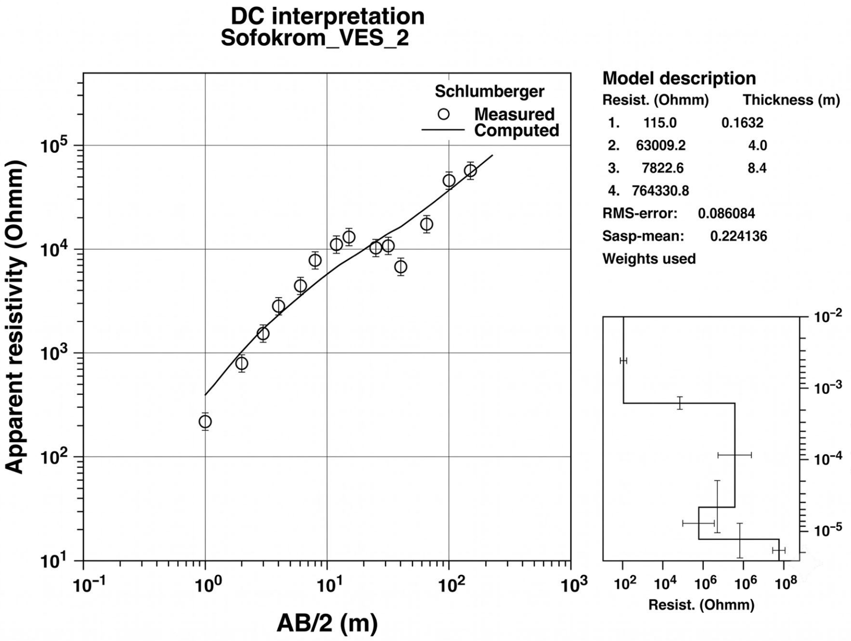

Figure 16. Depth sounding curve and 1D lithologic profile at VES_2 location.

At the VES 3 location (644991E/551409N, ELEV = 48 m), the characteristic sounding curve shows an HA-type curve with 4 geoelectric layers (Figure 17). The topsoil has a resistivity value of 2928 Ohm-m and a thickness of 0.21 m. The second layer's resistivity was estimated to be 447 Ohm-m with a thickness of 0.37 m, while the third layer is characterised by a resistivity value of 75,834 Ohm-m and thickness of 0.55 m. The bedrock resistivity was estimated to be 100,000 Ohm-m, depicting an infinitely resistive medium, while the overburden was estimated at 1.13 m. The shallowness of the depth of probing could be attributed to the erratic changes in the resistivity of the highly resistive rock formation underlying the site.

Results of the resistivity sounding carried out at the VES 4 location (645042E/551389N, ELEV = 57 m) are shown in Figure 18, whereby an AA-type curve depicting an increasing resistivity with depth over for 4-layer derived earth model. The resistivity of the topsoil was estimated to be 447 Ohm-m with a thickness of 0.19 m, while the underlying layer has a resistivity value of 11,104 Ohm-m and thickness of 0.51 m. The third layer has a resistivity value of 137,167 Ohm-m and a thickness of 2.2 m. The underlying bedrock resistivity was estimated as 8835401 Ohm-m with overburden thickness estimated to be 2.9 m. The high resistivity values are interpreted to reflect relatively dry and competent subsurface materials that may also have undergone significant weathering and leaching. Since electrical resistivity is a non-unique property, these interpretations are strengthened by the trial pit observations and laboratory geotechnical results rather than being inferred solely from resistivity values.

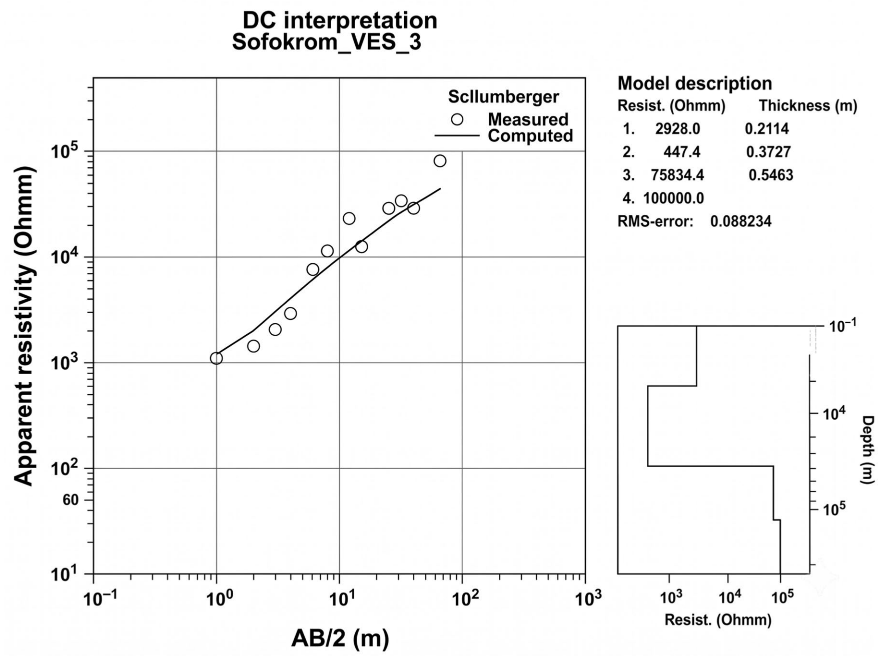

Figure 17. Depth sounding curve and 1D lithologic profile at VES_3 location.

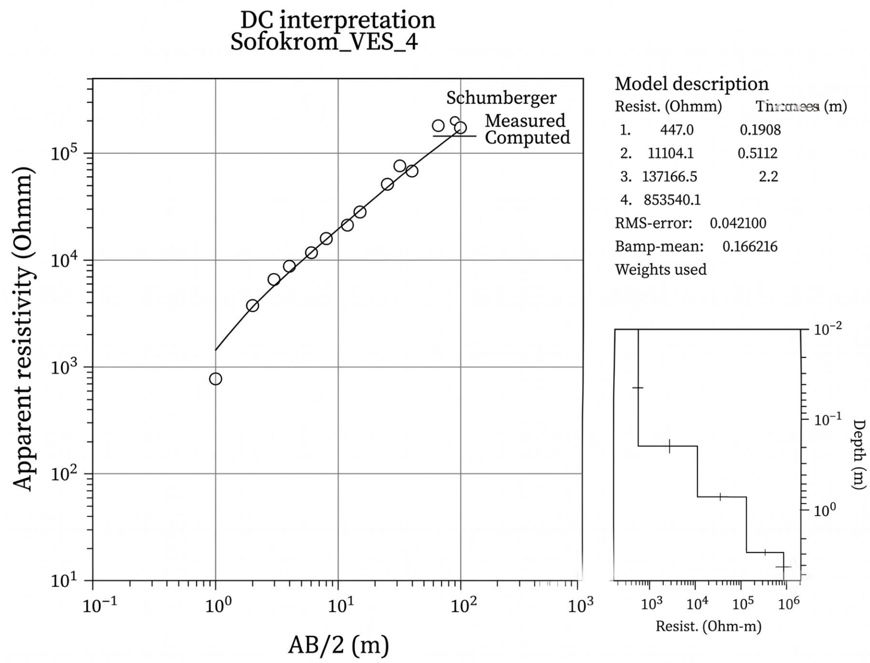

Figure 18. Depth sounding curve and 1D lithologic profile at VES_4 location.

Figure 19 shows the characteristic AA-type resistivity curve diagnostic of a rising resistivity trend over a 4-layer lithologic profile under VES 5 location 5 (645047E/551369N, ELEV = 49 m). The topsoil is characterised by a resistivity of 109 Ohm-m diagnostic of wet sand having a thickness of 0.11 m, while the underlying layer resistivity is 203,787 Ohm-m and thickness of 5.4 m. The third layer resistivity value was estimated to be 451,763 Ohm-m with a thickness of 20.2 m.

Bedrock is extremely resistivity with a value of 1,000,000 Ohm-m, while overburden thickness at the location was estimated at 25.71 m.

The geoelectric section and resistivity profile obtained at VES 6 (645098E/551571N, ELEV = 62.5 m) location are displayed in Figure 20, where 4-layer lithologic units were encountered. The derived AA-resistivity curve shows that the topsoil has a resistivity value of 107 Ohm-m and thickness of 0.10 m, while layer 2 has a resistivity value of 5929 Ohm-m and thickness of 0.17 m. Third-layer resistivity was estimated to be 35,239 Ohm-m with a thickness of 0.38 m. The overburden thickness was calculated to be 0.65 m, while the bedrock resistivity was estimated to be 100,000 Ohm-m. The resistivity pattern suggests relatively dry and competent overburden materials overlying a highly resistive sandstone unit. However, because similar resistivity values may arise from different geological conditions, the interpretation is corroborated by the lithological information obtained from the trial pits and laboratory analyses.

Figure 21 shows both the results of interpretation conducted for the VES data from the VES 7 location (645080E/551313N, ELEV = 57.5 m), showing the inverted 1D resistivity curve and the lithologic profile that revealed an HA-type geoelectric model. The resistivity profile indicated thin topsoil having a resistivity value of 10,004 Ohm-m and a thickness of 0.49 m, while the underlying second layer has resistivity of 2932 Ohm-m with a thickness of 1.7 m. The third layer resistivity value is estimated to be 9338 Ohm-m with a thickness of 0.86 m. The bedrock at this location has a higher resistivity value of 32,033 Ohm-m while the overburden thickness is estimated as 3.5 m.

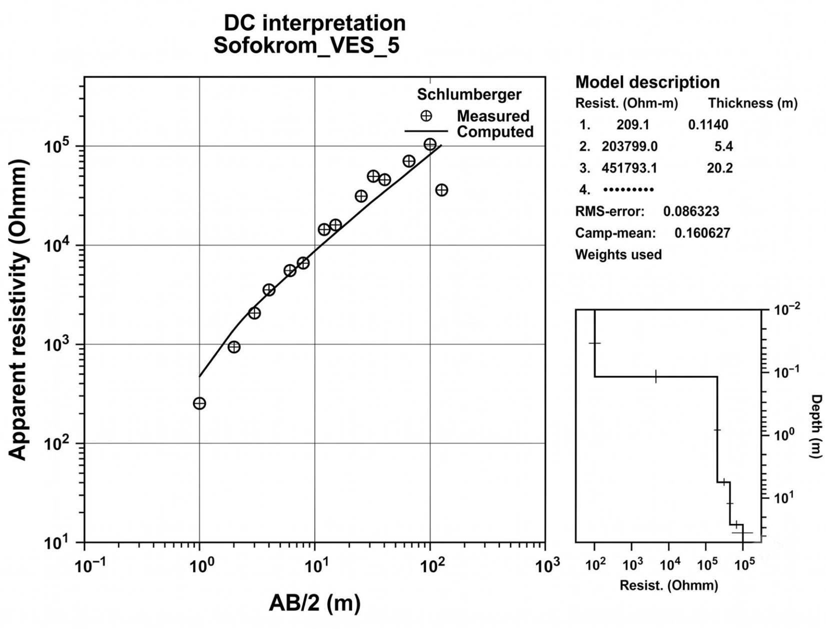

Figure 19. Depth sounding curve and 1D lithologic profile at VES_5 location.

The resistivity profile from the interpreted VES data at VES 8 location (645048E/

551286, ELEV = 45.5 m) depicts an AA-type curve indicating 4-layer lithologic units as shown in Figure 22. The topsoil is characterised by a resistivity value of 253 Ohm-m, having a thickness of 0.06 m, while the second layer resistivity was estimated at 4363 Ohm-m with a thickness value of 0.14 m. The third layer has a resistivity value of 15,875 Ohm-m and a thickness of 5.9 m. The bedrock resistivity was estimated to be 189,539 Ohm-m with the overburden thickness obtained to be 6.1 m.

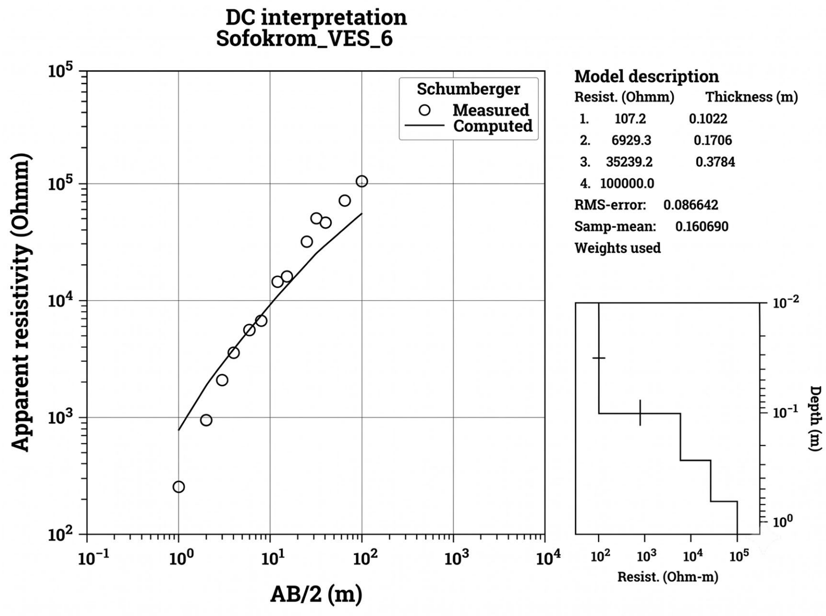

Figure 20. Depth sounding curve and 1D lithologic profile at VES_6 location.

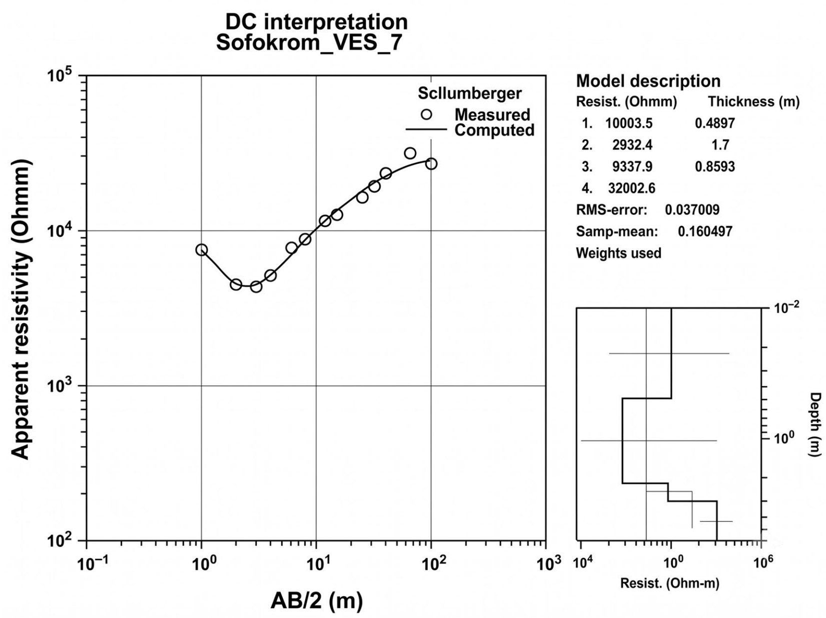

Figure 21. Depth sounding curve and 1D lithologic profile at VES_7 location.

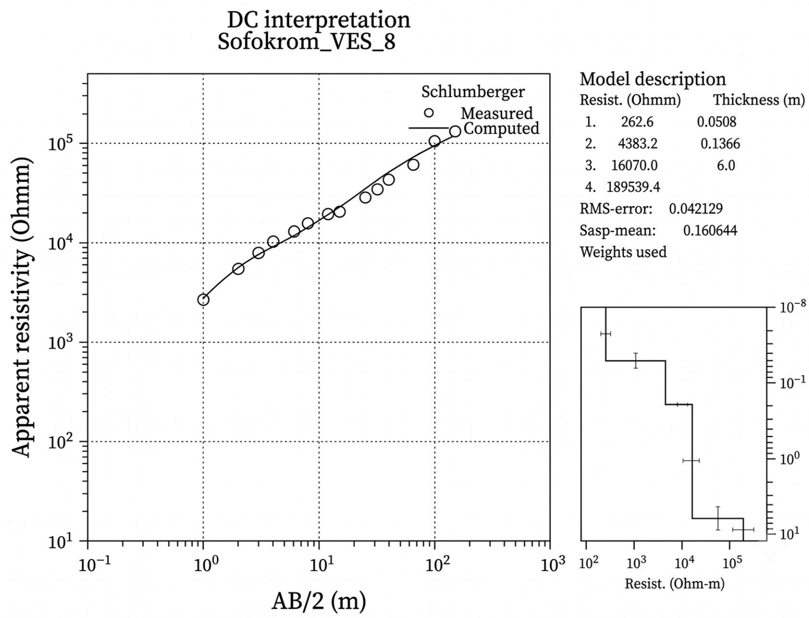

Figure 22. Depth sounding curve and 1D lithologic profile at VES_8 location.

4.2. Geotechnical Analysis

The geotechnical properties of the soil samples from five trial pits hand-dug to a depth of 1.5 m were investigated. The results from the various geotechnical tests conducted are discussed in the following sections and the material properties are presented in figures and tables. As shown in Figure 2, three of the pits (Pits 1, 2, and 3) were distributed on the hilly part towards the northern part of the study area, while sample Pits 4 and 5 were located at the slope section toward the southern part.

For engineering interpretation, the subgrade quality was assessed using an integrated evaluation of the AASHTO and USCS soil classifications, Atterberg limits, particle-size distribution, natural moisture content and shear strength characteristics. Materials classified as "good" subgrade exhibit favourable grading, relatively low plasticity and adequate engineering strength, whereas "fair" subgrade materials possess acceptable but comparatively lower engineering performance because of their grading and strength characteristics.

4.2.1. Derived Soil Profiles

It was discovered that three of the pits (Pits 1, 2, and 3) located on the hilly part have the same soil profile that is presented in Figure 23(a), while samples from Pits 4 and 5 obtained from the slope section also displayed the same soil profile shown in Figure 23(b). From the geological profiles in Figure 23 and a summary of the geotechnical results in Table 1, the trial Pits 1, 2 and 3 indicate stiff, dry brown, loose, and shattered coarse-grained sand silt mixtures (GC) up to a depth of 0.9 m. Similarly, soil samples from the trial Pits 4 and 5 compose of dry brown, loose, gravel-sand-silt mixtures (GM) from the ground level up to a depth of 0.9 m.

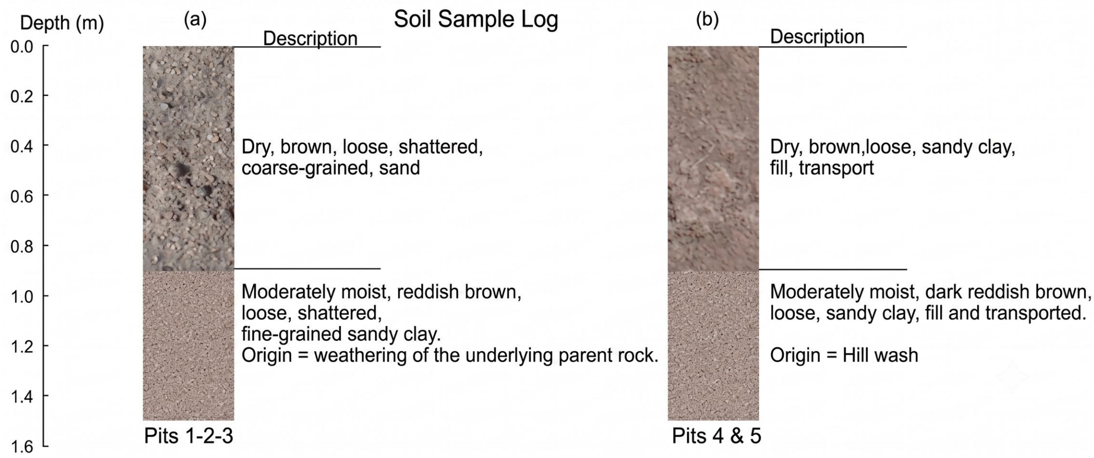

Figure 23. Soil profiles of the samples from the trial pits.

Table 1. Summary of geotechnical results.

Soil Sample Test		Pit 1	Pit 2	Pit 3	Pit 4	Pit 5	Average
Natural moisture content (NMC)		19.3%	20.3%	18%	16.1%	17.5%	18.24%
Liquid Limit		30%	29%	30%	25%	26%	28%
Plastic Limit		19%	20%	18%	16%	17%	18%
Plasticity Index		11%	9%	12%	9%	9%	10%
Plasticity Chart Classification		Intermediate Plasticity clay	Intermediate Plasticity clay	Intermediate Plasticity clay	Low Plasticity silt	Low Plasticity silt	Intermediate Plasticity silt
Particle size distribution	Clay	9.6%	8.6%	9.4%	7.2%	7.6%	8.41%
	Sand	12.8%	14%	14.6%	30%	27.8%	19.48%
	Gravel	77.6%	77.4%	76%	62.8%	64.6%	71.68%
Specific Gravity, g/cm^3		2.75	2.74	2.73	2.67	2.69	2.77
AASHTO		A-2-6	A-2-6	A-2-6	A-2-4	A-2-4	A-2-6
USCS		GC	GC	GC	GM	GM	GC
$C_u = \frac{D_{60}}{D_{10}}$		12.85	8.89	10	6	6.36	8.82
Major constituent		Gravel-sand-clay mixtures	Gravel-sand-clay mixtures	Gravel-sand-clay mixtures	Silty gravels	Silty gravels	Gravel-sand-clay mixtures

The average percentages of clay (8.48%), sand (19.84%) and gravel (71.25%) sum to approximately 99.57% because the individual particle-size fractions have been rounded to one decimal place. The small difference from 100% is therefore attributed to rounding and does not affect the soil classification. From a depth of 0.9 m to 1.5 m, the soil profile of trial Pits 1 - 3 reveals moderately moist, reddish brown, loose, shattered, fine-grained sandy clay showing clear signs of weathering. Trial Pits 4 and 5 at the flank of the undulating ridge were found to be moderately moist, dark-reddish brown, loose, sandy clay materials within a depth of 0.9 - 1.5 m that are believed to have been transported downslope from the adjacent ridge. The low PI values of the fines are also a pointer to their mineralogical makeup. This then suggests that the clay and silt minerals are likely micaceous sandstones [35], thus having a zero shrink-swell potential than other clay minerals.

4.2.2. Atterberg Limits

The Atterberg tests yield consistency limits that include Liquid Limits (LL), Plastic Limits (PL), and Plasticity Index (PI) for the tested soil samples from the various trial pits. **Table 1** shows the liquid limits varying between 25% and 30%, while the plasticity limit ranges from 16% - 20%. The plasticity index of the soil samples is found to be in the range of 8.5% - 12%. The relatively similar consistency in trial Pits 2, 4, and 5 suggests that the soil will behave similarly when extra water is added to them. The relatively low liquid limits and plasticity indices indicate soils with limited volume-change potential, thereby contributing to favourable subgrade performance under anticipated loading conditions. These consistency characteristics were considered together with the particle-size distribution and soil classification in evaluating the engineering suitability of the site.

4.2.3. Particle Size Distribution

The results of the particle size analyses conducted on the soil samples are also presented in **Table 1** whereby the grain size distribution and specific gravity interpolation above the mechanical sieving method revealed the soils' structures. From **Figure 24**, the plasticity chart shows that the soil samples from Pits 1, 2, and 3 fall above the A-Line, which results in the classification of the soils as GC (gravel-sand-clay mixtures). However, samples from Pits 4 and 5 fall below the A-Line, which results in these samples being classified as GM (gravel-sand-silt mixtures). The specific gravity of the soil samples ranges from 2.67 - 2.75 7 g/cm^3, showing similarities in textural and mineralogical composition that is typical of soils rich in quartz [36]. The low specific gravity of trial Pits 4 and 5 could be attributed to the dominance of angular particles in the soil and the low percentage of fine (clay) minerals in them [3] [35]. Based on the AASHTO and USCS classification systems, soil samples from trial Pits 1, 2 and 3 are classified as A-2-6 (GC), indicating gravelly soils with clay fines that are generally considered good subgrade materials because of their relatively low plasticity, high gravel content and favourable engineering characteristics. In contrast, trial Pits 4 and 5 are classified as A-2-4 (GM), representing silty gravel soils that are considered fair subgrade materials owing to their comparatively higher sand content and lower cohesion. The engineering assessment of subgrade quality was therefore based on the combined interpretation of the USCS classification, AASHTO classification, particle-size distribution, plasticity characteristics and direct shear strength results rather than on a single engineering parameter.

4.2.4. Results of Direct Shear Test

The direct shear test was also conducted on representative soil samples from trial Pits 3 and 4 to determine the shear strength, the ultimate bearing capacity, and the allowable bearing capacity of the subgrade materials to withstand applied loads before failing in shear. Graphical representations of the relationships between the shear stress and displacement experienced under applied load for the soil samples were produced. From the graphs, the peak shear stress values of the various loads applied were plotted against measured normal stress, and the curves were extrapolated to determine the soils' Cohesions.

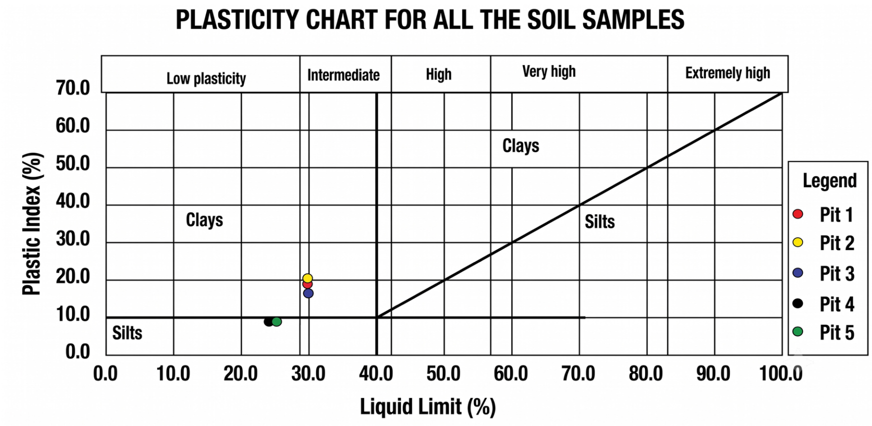

Figure 24. Plasticity plot for the soil samples from the trial pits.

Table 2. Derived parameters from direct stress test conducted for the representative sample from Pit 3.

<table>
<tr><th>Normal load (kg)</th><th>Normal Stress (KN/m²)</th><th>Shear Stress (KN/m²)</th><th></th></tr>
<tr><td>2.1</td><td>5.725</td><td>13.432</td><td></td></tr>
<tr><td>4.2</td><td>11.445</td><td>20.814</td><td></td></tr>
<tr><td>8.5</td><td>23.163</td><td>23.655</td><td></td></tr>
<tr><td colspan="4">Estimation of Bearing Capacity</td></tr>
<tr><td>Width of footing (B), (m)</td><td>Length of footing (L), (m)</td><td>Depth of footing (D), (m)</td><td rowspan="2">Cohesion (C) = 12.1038 (kN/m²)
Angle of friction (Ø) = 31.2˚
Unit Weight = 17.240 kN/m²</td></tr>
<tr><td>2</td><td>4</td><td>1.5</td></tr>
<tr><td colspan="4">Bearing Pressure Factors</td></tr>
<tr><td>N_C</td><td>N_q</td><td>N_λ</td><td rowspan="2">Ultimate Bearing Capacity,
qr = 1552.7 kN/m²
Allowable Bearing Capacity,
qa = 480.6 kN/m²</td></tr>
<tr><td>40.411</td><td>25.282</td><td>22.650</td></tr>
</table>

For the representative sample from Pit 3 from the hilly part of the site, Figure 25 shows the plot of the shear stress against displacement under the various load capacity, while Table 2 shows the parameters from the test results employed in deriving the bearing capacities and soil cohesion of the representative sample.

Analysis of the direct shear test results shows that the representative sample has a cohesion of 12.1038 kN/m^2 (**Figure 26**) and an internal friction angle of 31˚. The ultimate bearing capacity of the soil is 1552.7 kN/m^3 and the allowable bearing capacity that the soil can withstand is 480.6 kN/m^3. From **Table 2**, the measured shear strength of the representative soil sample from trial Pit 3 ranges from 13.43 to 23.66 kPa. According to the shear-strength classification presented in **Table 3**, these values span the very low (10 - 20 kPa) and low (20 - 40 kPa) categories. This indicates that the soil exhibits very low to low undrained shear strength and, although it possesses appreciable bearing capacity, foundation design should explicitly consider the measured shear-strength parameters together with the integrated geophysical and geotechnical site conditions, suggesting that the soil possesses relatively low shear strength and that foundation design should account for the measured strength parameters together with the geophysical interpretation and site-specific loading conditions.

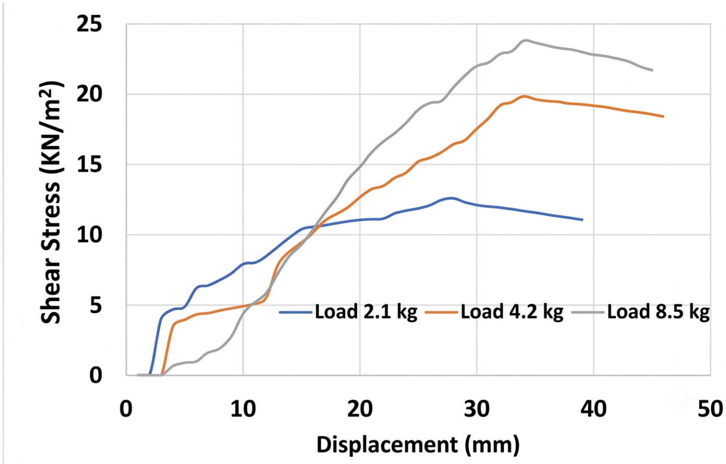

Figure 25. Graphical display of shear stress against displacement for representative sample from trial Pit 3.

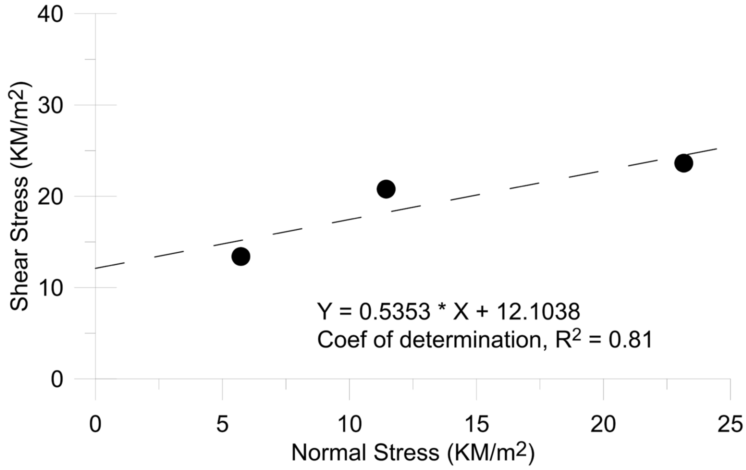

Figure 26. Plot of peak shear stress against measured normal stress for representative sample from Pit 3.

Table 3. Shear strength classification (BS EN ISO 14688-2:2004, 5.3).

Term Based on Measurement	Undrained Shear Strength Classification (KPa)
Extremely low	<10
Very low	10 - 20
Low	20 - 40
Medium	40 - 75
High	75 - 150
Very high	150 - 300

The graph of the plot of shear stress against displacement under the various load capacity for the representative sample from Pit 4 on the slope part southward is displayed in **Figure 27** and **Table 4** shows the various parameters from the test results employed in deriving bearing capacities and soil cohesion (**Figure 28**). The analysis of the direct shear test results on the soil sample from Pit 4 indicated that it has a cohesion of 9.6796 kN/m^2 and an internal friction angle of 28.97˚. The ultimate bearing capacity of the soil is estimated to be 1281.7 kN/m^3, while the allowable bearing capacity that the soil can withstand is 410.3 kN/m^3.

The measured shear strength of the representative soil sample from trial Pit 4 ranges from 11.20 to 20.45 kPa. Based on the classification presented in **Table 3**, these values fall within the very low to low undrained shear-strength categories. This indicates comparatively weaker near-surface materials within the slope/depression zone relative to the hilly terrain, suggesting that appropriate foundation design and, where necessary, local ground improvement measures should be considered for heavily loaded structures.

Details of the geo-parameters obtained from the results of engineering geophysical and geological surveys conducted are summarized in **Figure 29** and **Figure 30**, whereby **Figure 29** displays the Ven diagram that gives 3D view of soil stratigraphy underlying the study area and **Figure 30** shows the columnal presentation of the geo-parameters, which can assist in the design of appropriate foundations for proposed infrastructures in the study area.

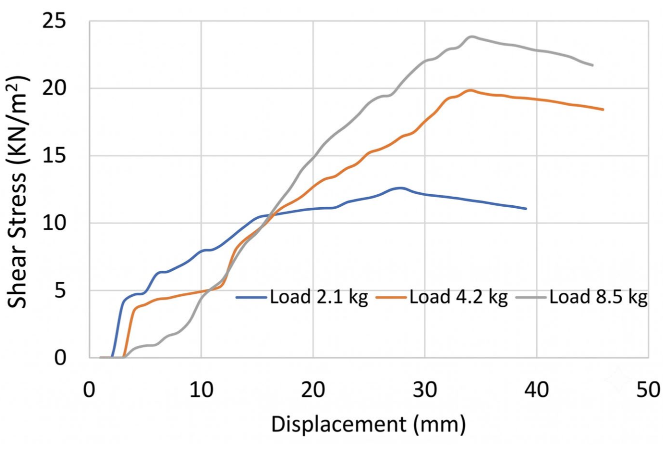

Figure 27. Graphical display of shear stress against displacement for representative sample from Pit 4.

Table 4. Derived parameters from direct stress test conducted for the representative sample from Pit 4.

Normal load (kg)	Normal Stress (KN/m^2)	Shear Stress (KN/m^2)	
2.1	5.723	11.200	
4.2	11.445	17.245	
8.5	23.163	20.450	
Estimation of Bearing Capacity			
Width of footing (B), (m)	Length of footing (L), (m)	Depth of footing (D), (m)	Cohesion (C) = 9.6796 (kN/m^2) Angle of friction (Ø) = 28.97˚ Unit Weight = 17.24 kN/m^2
2	4	1.5	
Bearing Pressure Factors			
N_C	N_q	$N\lambda$	Ultimate Bearing Capacity, qr = 1281.7 kN/m^2 Allowable Bearing Capacity, qa = 410.3 kN/m^2
34.242	19.981	16.18	

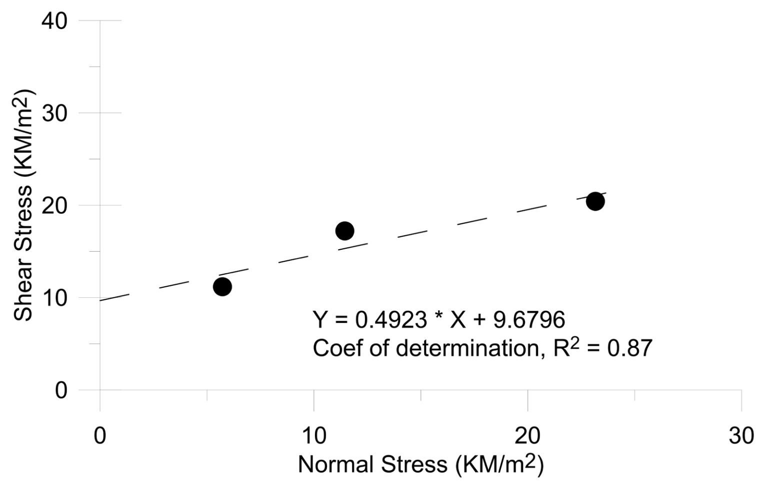

Figure 28. Plot of peak shear stress against measured normal stress for representative sample from Pit 4.

Figure 30 reveals that while the subgrade materials in northern and central parts are far above the water table, the depressed section where Pit 4 is located is close to the water table and this is the reason why fruit crops are able to grow in the gully at the southern edge of the study area. In all, the integrated geophysical and geotechnical investigations indicate that the site is generally underlain by competent subsurface materials capable of supporting civil infrastructure. However, localized depressions, fractured zones and areas of elevated moisture content may adversely affect foundation performance. Accordingly, foundation selection should be site-specific, with shallow foundations being suitable in competent areas, while localized ground improvement or deeper foundation systems may be required within weaker zones identified by the integrated investigation.

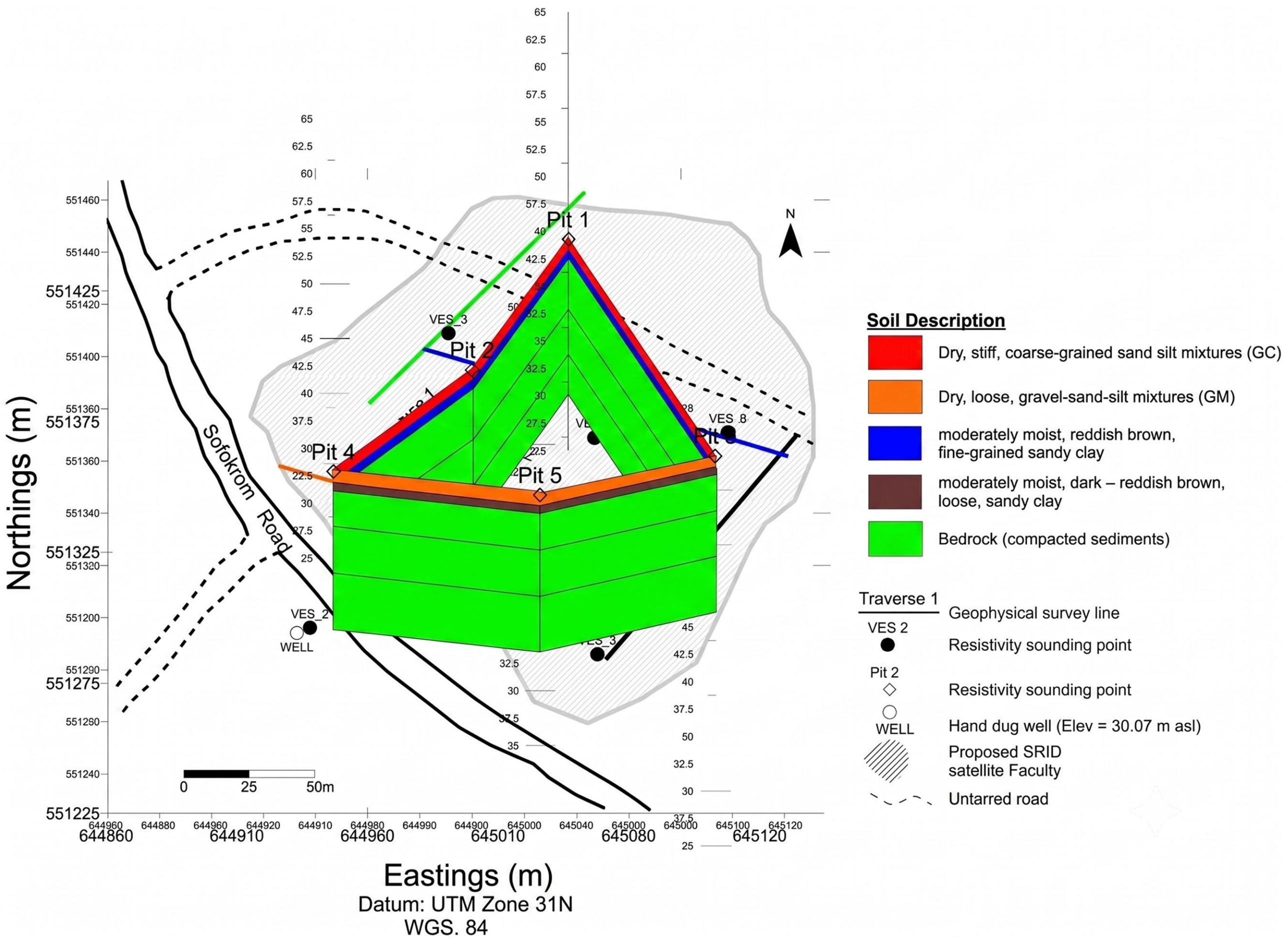

Figure 29. Ven diagram showing 3D view of the soil stratigraphy in the study area.

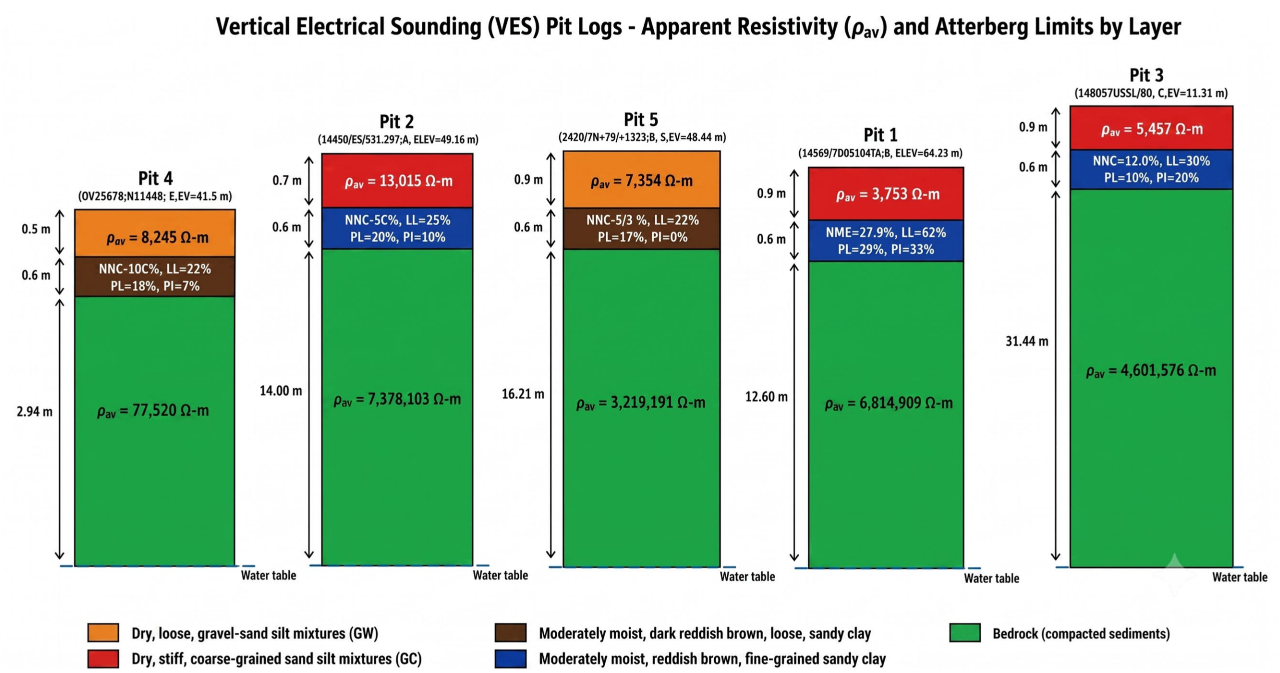

Figure 30. Columnal presentation of the geo-parameters for the lithologic sequence in the study area.

5. Conclusions

In this study, both engineering geophysical and geologic methods have been used in evaluating the integrity and competency of the subgrade materials in the study area for effective planning for infrastructural development. The integration of the two methods provides relevant geotechnical parameters for foundation works at the study area in terms of information on geophysical, hydrological, and geotechnical parameters that can assist in decision-making during the planning of civil engineering works at the site. The information provided includes physical characteristics of the subgrades (resistivity and thickness), consistency limits (liquid limits and plasticity index) of the subgrade, water table, subgrades' specific gravity, and underlying bedrock geologic structures that might have an influence on the stability of erected structures at the site.

Both the 2D electrical resistivity imaging and Vertical Electrical Sounding (VES) surveys revealed generally high resistivity values across much of the site, indicating relatively competent overburden and shallow bedrock. However, because electrical resistivity is a non-unique geophysical property, interpretations relating to weathering, moisture conditions and engineering competence were corroborated using trial pit logs and laboratory geotechnical test results. The integrated results indicate that the overburden is generally thin and competent, with localized depressions, fractures and seepage pathways that may reduce foundation stability in some parts of the site. The electrical resistivity imaging showed that the original topsoil is generally thin, particularly over the elevated portions of the site where erosion has exposed the underlying weathered materials. The observed resistivity variations are interpreted to reflect differences in lithology, moisture content, degree of weathering and topography rather than a single controlling factor.

The site, which rises above most places in Sofokrom Town, is also characterized by a highly resistive overburden that mimics underlying bedrock relief greatly. The overburden that forms the typical foundation layer has a thickness generally less than 5 m, except in zones of depression. It was observed that faulted layer is not pronounced in the area, but a series of joints, fractures, and localized depressions exist across the overburden through which surface water can easily percolate into the compacted bedrock. However, the occurrence of depression zones along traverses 3 and 4 at the far eastern and southern boundaries of the site leads to the gulley caused by possibly prolonged downpours during the rainy seasons. It was discovered that the closeness of the bedrock to the water table (30.07 m) at the southern part of the site might have increased the water content in the geologic section along traverse 4.

The resistivity soundings conducted show geoelectric profiles indicating weathering profiles typified by a 4-layer lithologic sequence characterised predominantly by AA-type (62.5%) diagnostic of stepwise rising in resistivity with depth. Other resistivity curves are KH (25%) and HA (12.5%). The AA-type curves are characterised by topsoil resistivity ranging from 107 - 447 Ohm-m with a layer thickness of 0.05 - 0.3 m. The second layer is characterised by resistivity values varying between 4363 Ohm-m and 203,987 Ohm-m and thickness ranging from 0.13 - 5.4 m. The third layer resistivity for the AA-type curve lies between 15,875 Ohm-m and 451,783 Ohm-m, while the layer thickness varies from 0.38 - 20.2 m. The bedrock resistivity values for this curve (AA-type) were estimated to vary from 105 - 106 Ohm-m (highly resistive medium).

The geophysical surveys indicate that the site is characterized by generally high resistivity values extending from the near surface to the investigated depth, suggesting relatively competent overburden underlain by resistive bedrock. These interpretations are supported by the trial pit observations and laboratory geotechnical results.

From the sample logs, the upper layer parts of soils from Pits 1, 2 and 3 on the hilly area are characterised by stiff, dry brown, loose, and shattered coarse-grained sand silt mixtures (GC) up to a depth of 0.9 m, while from a depth of 0.9 m to 1.5 m the soil materials from Pits 1, 2 and 3 are of moderately moist, reddish brown, loose, shattered, fine-grained sandy clay showing clear signs of weathering. Similarly, along the slope southward of the site, the soil samples from trial Pits 4 and 5 are composed of dry brown, loose, gravel-sand-silt mixtures (GM) from the ground level up to a depth of 0.9 m. Below this section, the soil materials were found to be moderately moist, dark-reddish brown, loose, sandy clay materials within a depth of 0.9 - 1.5 m that are believed to be transported down the hill. It was discovered that the underlying sub-soil materials are predominantly part of underlying bedrock made up of leached, moderately moist, and dark brown loose sandy clay, suggesting deep weathering of underlying bedrock. The saprolites are believed to have formed as part of the underlying bedrock that is associated with the Birimian Supergroup.

The low PI values of the fines are suggesting that the clay and silt minerals are likely micaceous sandstones [35], thus having a zero shrink-swell potential than other clay minerals. Based on the combined interpretation of the USCS and AASHTO soil classifications, particle-size distribution, Atterberg limits and shear-strength characteristics, the soils from trial Pits 1, 2 and 3 are classified as good subgrade materials. In contrast, the soils from trial Pits 4 and 5 are classified as fair subgrade materials because of their relatively lower cohesion and higher proportion of sandy and silty materials.

In the northern parts, across the hilly section, the soil materials are characterised by an average cohesion value of 12.1038 kN/m^2 and an internal friction angle of 31, while the ultimate bearing capacity is 1552.7 kN/m^3, and the allowable bearing capacity that the subgrade materials can withstand in the area is 480.6 kN/m^3. The measured shear strength of the soils on the hilly section ranges from 13.43 to 23.66 kPa, corresponding to the very low to low undrained shear-strength classes according to BS EN ISO 14688-2:2004. Nevertheless, the calculated bearing capacities indicate that the soils are capable of supporting structural loads when appropriate foundation designs are adopted. Similarly, the direct shear test results for soils at the slope area, southward of the site, exhibit a cohesion of 9.6796 kN/m^2 with an internal friction angle of 28.97, while the ultimate bearing capacity of the soil is estimated to be 1281.7 kN/m^3. For the soils in the slope where the subgrade materials are found to be transported down the hill, the allowable bearing capacity that the soil can withstand is 410.3 kN/m^3. The measured shear strength of the soils in the slope area ranges from 11.20 to 20.45 kPa, corresponding to the very low to low undrained shear-strength classes. Consequently, localized ground improvement or appropriate foundation design should be considered where heavy structural loads are anticipated.

The water table (30.07 m asl) is far below the overburden that can serve as subgrades; thus, it is believed that the water level might not pose any serious threat to the structural foundation at the site. Although the overburden materials generally possess suitable engineering properties and adequate bearing capacity, localized depressions, fractured zones and seepage pathways identified from the integrated geophysical and geotechnical investigations require site-specific foundation design. Cutting and filling operations, together with localized ground improvement where necessary, are recommended to provide stable foundation conditions. Likewise, stepping the foundation for the structures to be erected could also give aesthetic value to the infrastructures to be sited within the study area.

The integrated application of electrical resistivity imaging, Vertical Electrical Sounding and geotechnical investigations proved effective for characterizing the subsurface conditions at the site. While VES provided valuable information on vertical layering, the 2D electrical resistivity imaging more effectively resolved localized fractures, depressions and seepage pathways that are critical for engineering site characterization. Future investigations within the Sekondi-Takoradi area should therefore adopt an integrated geophysical and geotechnical approach to improve the reliability of foundation assessments and infrastructure planning.

Acknowledgements

The authors wish to acknowledge the assistance provided by the staff in the geotechnical laboratory of the Department of Geological Engineering, UMaT, Prof. Yakubu Isaka, and other staff of SRID for the assistance rendered during and after data acquisition at the site.

Conflicts of Interest

The authors declare no conflicts of interest regarding the publication of this paper.

References

[1] Woodward, J. (2005) An Introduction to Geotechnical Processes. Spon Press, 328 p.

[2] Das, B.M. (2010) Principles of Geotechnical Engineering. 7th Edition, PWS Publishing Company.

[3] Bowels, J.E. (1992) Engineering Properties of Soils and Their Measurements. 4th Edition, McGraw-Hill, 53-58.

[4] Kortatsi, B.K. (1994) Groundwater Utilization in Ghana. In: Soveri, J. and Suokko, T., Eds.,*Future Groundwater Resources at Risk*: *Proceedings of the Helsinki Conference*, IAHS Press, 149-156.

[5] Yidana, S.M., Alfa, B., Banoeng-Yakubo, B. and Obeng Addai, M. (2012) Simulation of Groundwater Flow in a Crystalline Rock Aquifer System in Southern Ghana—An Evaluation of the Effects of Increased Groundwater Abstraction on the Aquifers Using a Transient Groundwater Flow Model. *Hydrological Processes*, **28**, 1084-1094. https://doi.org/10.1002/hyp.9644

[6] Look, B.G. (2007) Handbook of Geotechnical Investigation and Design Tables. Taylor and Francis, 356 p.

[7] Telford, W.M., Geldart, L.P., Sheriff, R.E. and Keys, D.A. (1990) Applied Geophysics. 2nd Edition, Cambridge University Press, 344-536.

[8] Kearey, P., Brooks, M. and Hill, I. (2002) An Introduction to Geophysical Exploration. 3rd Edition, Blackwell Science Ltd, 262 p.

[9] Neil, A. and Ahmed, I.A. (2006) Generalized Protocol for Selecting Appropriate Geophysical Techniques. Departments of Geology and Geophysics, University of Missouri-Rolla. 19 p.

[10] Loke, M.H. (2001) Tutorial: 2-D and 3-D Electrical Imaging Surveys. 128 p. https://sites.ualberta.ca/~unsworth/UA-classes/223/loke_course_notes.pdf

[11] Ibitoye, F.P., Ipinmoroti, F.V., Salami, M., Akinluwade, K.J., Taiwo, A.T. and Adetunji, A.R. (2013) Application of Geophysical Methods to Building Foundation Studies. *International Journal of Geosciences*, **4**, 1256-1266. https://doi.org/10.4236/ijg.2013.49120

[12] Foster, M.P. and Evans, A.N. (2008) An Evaluation of Interpolation Techniques for Reconstructing Ionospheric TEC Maps. *IEEE Transactions on Geoscience and Remote Sensing*, **46**, 2153-2164. https://doi.org/10.1109/tgrs.2008.916642

[13] Soupios, P.M., Georgakopoulos, P., Papadopoulos, N., Saltas, V., Andreadakis, A., Vallianatos, F., *et al*. (2007) Use of Engineering Geophysics to Investigate a Site for a Building Foundation. *Journal of Geophysics and Engineering*, **4**, 94-103. https://doi.org/10.1088/1742-2132/4/1/011

[14] Reynolds, J.M. (1997) An Introduction to Applied and Environmental Geophysics. John Willey and Sons, 796 p.

[15] Roth, M.J.S., Mackey, J.R., Mackey, C. and Nyquist, J.E. (2002) A Case Study of the Reliability of Multielectrode Earth Resistivity Testing for Geotechnical Investigations in Karst Terrains. *Engineering Geology*, **65**, 225-232. https://doi.org/10.1016/s0013-7952(01)00132-6

[16] Abidin, H.Z., Andreas, H., Gumilar, I., Fukuda, Y., Pohan, Y.E. and Deguchi, T. (2011) Land Subsidence of Jakarta (Indonesia) and Its Relation with Urban Development. *Natural Hazards*, **59**, 1753-1771. https://doi.org/10.1007/s11069-011-9866-9

[17] Nascimento da Silva, C.C., de Medeiros, W.E., Jardim de Sá, E.F. and Neto, P.X. (2004) Resistivity and Ground-Penetrating Radar Images of Fractures in a Crystalline Aquifer: A Case Study in Caiçara Farm—Ne Brazil. *Journal of Applied Geophysics*, **56**, 295-307. https://doi.org/10.1016/j.jappgeo.2004.08.001

[18] Abroampah, M.P., Boakye, E. and Yalley, P.P. (2015) The Impact of Sofokrom Quarry on River Anankwari. *International Journal of Scientific Research* (*IJSR*), **4**, 1057-1062.

[19] Anon (2025) Ghana Climate Vulnerability Hub Sekondi Takoradi. https://ghclimatevulnerabilityhub.com/sekondi/profile-details.php?id=17

[20] Atta-Peters, D. (1999) Upper Devonian Acritarchs from the Lower Takoradi Shales of the Sekondian Group. *Ghana Mining Journal*, **5**, 1-10.

[21] Odjer-Bio, N.T., Belford, E.J.D. and Ansong, M. (2015) What Is Happening to Our Lagoons? The Example of Butuah Lagoon in Ghana. *International Journal of Energy and Environmental Engineering*, **6**, 183-193. https://doi.org/10.1007/s40095-015-0165-1

[22] Fei-Baffoe, B., Nyankson, E.A. and Gorkeh-Miah, J. (2014) Municipal Solid Waste Management in Sekondi-Takoradi Metropolis, Ghana. *Journal of Waste Management*, **2014**, Article ID: 823752. https://doi.org/10.1155/2014/823752

[23] Asiedu, D., Atta-Peters, D., Hegner, E., Hegner, A. and Shibata, T. (2011) Palaeoclimatic Control on the Composition of Palaeozoic Shales from Southern Ghana, West Africa. *Ghana Mining Journal*, **12**, 7-16. https://doi.org/10.4314/gm.v12i1.64364

[24] Hodgson, P.N. (2011) Social Acceptance as Guidance for Permitting Quarries in Ghana: A Case Study of Sekondi-Takoradi Metropolis. Ph.D. Thesis, University of Cape Coast.

[25] Asiedu, D.K., Hegner, E., Rocholl, A. and Atta-Peters, D. (2005) Provenance of Late Ordovician to Early Cretaceous Sedimentary Rocks from Southern Ghana, as Inferred from Nd Isotopes and Trace Elements. *Journal of African Earth Sciences*, **41**, 316-328. https://doi.org/10.1016/j.jafrearsci.2005.05.003

[26] Ankah, M.L.Y., Frimpong, R.A., Odum, E.K., Meten, M. and Klu, A.K. (2025) Landslide Susceptibility Mapping Using GIS-Based Logistic Regression Model in Sekondi-Takoradi Metropolitan Area of Ghana. *Discover Applied Sciences*, **7**, Article No. 1009. https://doi.org/10.1007/s42452-025-07147-2

[27] Danso, S.Y. and Addo, I.Y. (2017) Coping Strategies of Households Affected by Flooding: A Case Study of Sekondi-Takoradi Metropolis in Ghana. *Urban Water Journal*, **14**, 539-545. https://doi.org/10.1080/1573062x.2016.1176223

[28] Martines-López, J., Rey, J., Dueñas, J., Hidalgo, C. and Benavente, J. (2013) Electrical Tomography Applied to the Detection of Subsurface Cavities. *Journal of Cave and Karst Studies*, **75**, 28-37. https://doi.org/10.4311/2011es0242

[29] BS 1377: Part 2 (1990) British Standard Methods of Test for Soils for Civil Engineering Purposes, Part 2: Specific Gravity. British Standards Institution, 35-55.

[30] Alakuventhan, V. (2014) An Investigation on the Use of Oedometer Method for Determination of Liquid Limit Value of Soil. Bachelor Thesis, University of Malaysia, Pahang.

[31] Casagrande, A. (1948) Classification and Identification of Soil. *Transactions of the American Society of Civil Engineers*, **113**, 901-930. https://doi.org/10.1061/taceat.0006109

[32] Andrade, F.A., Al-Qureshi, H.A. and Hotza, D. (2011) Measuring the Plasticity of Clays: A Review. *Applied Clay Science*, **51**, 1-7. https://doi.org/10.1016/j.clay.2010.10.028

[33] Haigh, S. (2016) Consistency of the Casagrande Liquid Limit Test. *Geotechnical Testing Journal*, **39**, 13-19. https://doi.org/10.1520/gtj20150093

[34] Hazelton, P. and Murphy, B. (2016) "Interpreting Soil Test Results", What Do All the Numbers Mean? CSIRO Publishing.

[35] Budhu, M. (2010) Soil Mechanics and Foundation. 3rd Edition, John Wiley & Sons Inc.

[36] Roy, S. and Bhalla, S.K. (2017) Role of Geotechnical Properties of Soil on Civil Engineering Structures. *Resources and Environment Journal*, **7**, 103-109.